Heat Transfer in a High-pressure Gas-solid Fluidized Bed with Horizontal Tube Bundle and Continuous Addition of Fines

by
Fang Li

A thesis submitted in partial fulfillment of the requirements for the
Master's degree in Applied Science

Department of Chemical and Biological Engineering
Faculty of Engineering
University of Ottawa

Abstract

Climate change is becoming more severe than ever in human history and the emission of green house gas urgently needs to be reduced while global energy consumption remains booming. Large-scale application of clean fossil fuel combustion shall be considered as a priority for its economical advantages as well as reliability in meeting global energy needs. Oxygen-fired pressurized fluidized bed combustor technology with downstream carbon capture and sequestration is considered a key approach to clean coal combustion. In such technology, the fluidized bed combustor operates at elevated pressures and houses an in-bed heat exchanger tube bundle. It is essential to understand the rate of heat transfer between the immersed heat exchange surface and the fluidized bed as it is a key parameter in heat exchanger design. The goal of this work was to investigate the impact of pressure and presence of fine particles (i.e., surrogate for pulverized fuel) on the overall tube-to-bed heat transfer coefficient.

Experiments were conducted in a pilot-scale fluidized bed with an inner diameter of 0.15 m under cold flow conditions. A tube bundle consisting of five horizontal staggered rows was completely submerged in the bed. One of the tubes was replaced by a heating cartridge housed in a hollowed copper rod. Five thermocouples distributed at 45º intervals along the copper rod circumference measured the surface temperature and ensured that local effects were included. The bed material was large glass beads of 1.0 mm in diameter while the fines were glass beads of 60 μm in diameter and thus susceptible to entrainment. The fine particles were continuously fed to the fluidized bed and then captured downstream by a filter system. Fluidization was conducted at 101, 600 and 1200 kPa with excess gas velocities (U_g - U_{mf}) of 0.21, 0.29 and 0.51 m/s. Fine particle feed rates were 0, 9.5 and 14.4 kg/h. Two heating rod positions (2^{nd} row and 4^{th} row) were studies.

Overall, the heat transfer coefficient approximately doubled when pressure was increased from 101 to 1200 kPa. At atmospheric conditions, where the slug flow regime occurred, the maximum heat transfer coefficient was at the bottom of the rod, while it moved to the side of the rod at high pressures where the bubbling regime occurred. As the heating rod moving from 2^{nd} row to the 4^{th} row, the averaged heat transfer coefficient increased by respectively 18%, 9% and 6% at 101, 600 and 1200 kPa. The addition of fine particles decreased the average heat transfer coefficient by 10 to 20 W/m^2 K where the time – averaged heat transfer coefficient was approximately 220 and 450 W/m^2K at 101 kPa and 1200 kPa respectively. There was no effect on the angular profile across the tube surface. The results showed that average heat transfer coefficients matched the correlation developed by Molerus et al. (1995) within a 5% difference across all conditions when fines were not present.

Résumé

Le changement climatique devient plus sévère que jamais dans l'histoire de l'humanité et les émissions de gaz à effet de serre doivent être réduites d'urgence tandis que la consommation énergétique mondiale reste en plein essor. L'application à grande échelle de la combustion de combustibles fossiles propres doit être considérée comme une priorité pour ses avantages économiques ainsi que sa fiabilité pour répondre aux besoins énergétiques mondiaux. La technologie de combustion à lit fluidisé sous pression alimentée en oxygène et la capture et la séquestration du carbone en aval sont considérées comme une approche clé pour la combustion propre du charbon. Dans une telle technologie, la chambre de combustion à lit fluidisé fonctionne à des pressions élevées et loge un réseau de tubes d'échangeur de chaleur dans le lit. Il est essentiel de comprendre le taux de transfert de chaleur entre la surface d'échange de chaleur immergée et le lit fluidisé, car c'est un paramètre clé dans la conception de l'échangeur de chaleur. Le but de ce travail était d'étudier l'impact de la pression et de la présence de particules fines (c.-à-d., substitut pour le combustible pulvérisé) sur le coefficient global de transfert de chaleur d'un tube à l'autre.

Les expériences ont été conduites dans un lit fluidisé à l'échelle pilote avec un diamètre interne de 0,15 m dans des conditions d'écoulement à froid. Un réseau de tubes constitué de cinq rangées décalées horizontalement était complètement immergé dans le lit. L'un des tubes a été remplacé par une cartouche chauffante logée dans une tige de cuivre évidée. Cinq thermocouples répartis à des intervalles de 45º le long de la circonférence de la tige de cuivre mesuraient la température de surface et assuraient que les effets locaux étaient inclus. Le matériau du lit était de grosses billes de verre de 1,0 mm de diamètre tandis que les fines étaient des billes de verre de 60 μm de diamètre et donc susceptibles d'être entraînées. Les particules fines ont été continuellement introduites dans

le lit fluidisé et ensuite capturées en aval par un système de filtration. La fluidisation a été effectuée à 101, 600 et 1200 kPa avec des vitesses de gaz en excès (U_g - U_{mf}) de 0,21, 0,29 et 0,51 m/s. Les taux d'alimentation des particules fines étaient de 0, 9,5 et 14,4 kg/h. Deux positions de la tige chauffante (2^e rangée et 4^e rangée) ont été étudiées.

Globalement, le coefficient de transfert thermique a doublé lorsque la pression a été augmentée de 101 à 1200 kPa. Dans les conditions atmosphériques, où un régime d'écoulement en piston s'est produit, le coefficient maximum de transfert de chaleur se trouvait au bas de la tige, tandis qu'il se déplaçait vers le côté de la tige à des pressions élevées où le régime d'écoulement à bulles se produisait. Au fur et à mesure que la tige chauffante passait de la 2^e rangée à la 4^e rangée, le coefficient de transfert de chaleur moyen augmentait de 18%, 9% et 6% à 101, 600 et 1200 kPa, respectivement. L'ajout de particules fines a diminué le coefficient de transfert thermique moyen de 10 à 20 W/m^2K, où le coefficient de transfert de chaleur moyen est approximativement 220 and 450 W/m^2K à 101 kPa et 1200 kPa, respectivement. Il n'y avait aucun effet sur le profil angulaire à travers la surface du tube. Les résultats ont montré que les coefficients de transfert de chaleur moyens correspondent à la corrélation développée par Molerus et al. (1995) avec une différence de 5% dans toutes les conditions où les particule fines n'étaient pas présentes.

Table of Contents

List of Figures

List of Tables

Nomenclature

A	Heat transfer area; (m^2)
Ar	Archimedes number; (-)
d_B	Bubble diameter; (m)
C_D	Particle drag coefficient; (-)
c_p	Specific heat capacity; $\left(\frac{J}{kg\,K}\right)$
D	Diameter; (m)
D_C	Column inner diameter; (m)
E	Emissivity; (-)
f	Time fraction of contact; (-)
Fo	Fourier modulus; (-)
g	Gravitational acceleration; $\left(\frac{m}{s^2}\right)$
h	Global averaged heat transfer coefficient; $\left(\frac{W}{m^2K}\right)$
h_i	Local heat transfer coefficient; $\left(\frac{W}{m^2K}\right)$
$h_{rel,i}$	Local relative heat transfer coefficient; (-)
H	Static Bed Height; (m)
I	Current; (A)
k	Thermal conductivity; $\left(\frac{W}{mK}\right)$
Kn	Knudsen number for gas in particle-wall gap; (-)
P	Pressure; (kPa)
Pr	Prandtl number; (-)
q	Heat transfer rate; (W)
S_H	Horizontal pitch; (mm)
S_V	Vertical pitch; (mm)
T	Global averaged Temperature; (K)
T_i	Local averaged temperature at position i; (K)
T_i^*	Local instantaneous temperature at position i; (K)
$T_{rel,i}$	Local relative temperature; (-)
$T_{rel,i}^*$	Local relative instantaneous temperature at position i; (-)
U	Superficial gas velocity; $(\frac{m}{s})$

U_e	Excess superficial gas velocity over minimum fluidization; $\left(\frac{\mathrm{m}}{\mathrm{s}}\right)$
U_t	Particle terminal velocity; $(\frac{\mathrm{m}}{\mathrm{s}})$
V	Voltage; (V)
Greek Symbols	
ε	Void fraction; (-)
μ	Viscosity; $\left(\frac{\mathrm{kg}}{\mathrm{m\ s}}\right)$
ρ	Density; $\left(\frac{\mathrm{kg}}{\mathrm{m}^3}\right)$
τ	Contact time; (s)
σ	Standard deviation
δ	Bubble volume fraction; (-)
Subscripts	
ΔP	Differential Pressure
ΔT	Differential Temperature
b	Bed
C	Convective
$cond$	Conductive
$conv$	Convective
d	Dense phase
f	Fluid
l	Lean phase
mf	Minimum fluidization
p	Particle
pa	Packet
r	Radiative
t	Tube
W	Wall (submerged surface)

Acknowledgement

I owe my deep gratitude to my supervisor Dr Poupak Mehrani, and my co-supervisor Dr Arturo Macchi. I much appreciated that during the period of my study, they provided great patience, encouragement, enthusiasm and extremely professional advices. Without their continuous support, this study would have hardly been completed.

I want to thank Dr Robin Hughes from NRCan CanmetENERGY (Ottawa) and Dr Mark Fitzsimmons from Gas Technology Institute (USA) for their professional advices towards this project.

I am also deeply grateful to my group members, Di Song, Fahad Al Amin Chowdhury, Marc-André Olivier Séguin and Milad Taghavivand for their great and continuous support towards this project. I also want to thank the undergraduate students, Tushar Joshi and Bilal Elchamaa, for their help on performing the experiments. Special thanks to Eric Mielke, who guided me at the beginning of this study and kindly provided help so that I could start being involved into this project.

I would also like acknowledge the help from the staff at the Department of Biological and Chemical Engineering at the University of Ottawa: Franco Ziroldo, Gérard Nina, James Macdermid, Francine Pétrin and Sylvie Saindon for their kindness and assistance.

I would also like to thank the Natural Sciences and Engineering Research Council (NSERC) of Canada and NRCan CanmetENERGY-Ottawa for their financial supports.

Finally, I am extremly grateful to my family, my parents and my girlfriend for their love, understanding and constant support.

Chapter 1 Introduction

Climate change has widely raised concerns around the world. Clear evidences have shown that global warming is no longer a hypothesis, but reality [1]. According to NASA, Earth`s average temperature has increased roughly 2 degrees Fahrenheit during the 20th century [2]. Among those major global anthropogenic green-house gas (GHG) emissions by 2014 [3], energy generation contributed to 68% of GHG emissions whereas agriculture and industrial processes represented 12% and 5% of the emissions, respectively (Figure 1-1).

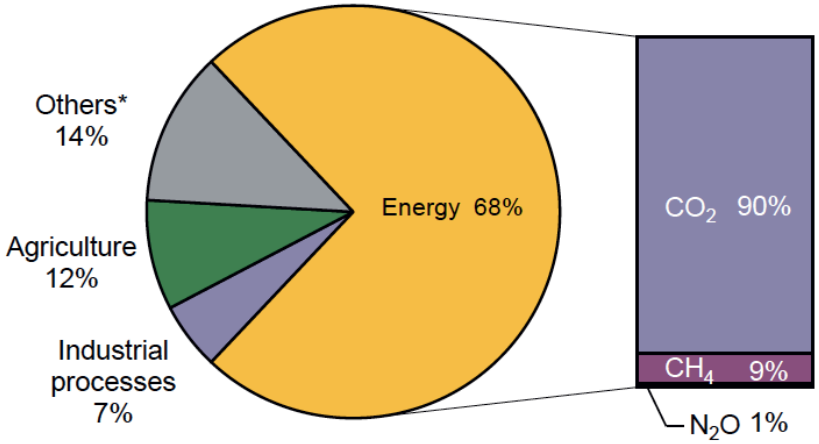

* Others include large-scale biomass burning, post-burn decay, peat decay, indirect N_2O emissions from non-agricultural emissions of NO_x and NH_3, Waste, and Solvent Use.

Figure 1-1: Estimated shares of contributors to the global anthropogenic GHG emissions published in 2014 [3]

Moreover, within the energy sector, CO_2 emitted from fuel combustion was the predominant contributor to the total GHG emissions. Another fact is that, in 2015, the majority of world primary energy supply was still from fossil fuels [3]. This is while the total energy supply nearly doubled from 1971 to 2015 (Figure 1-2), which indicated that the structure of energy supply among the world still remained similar.

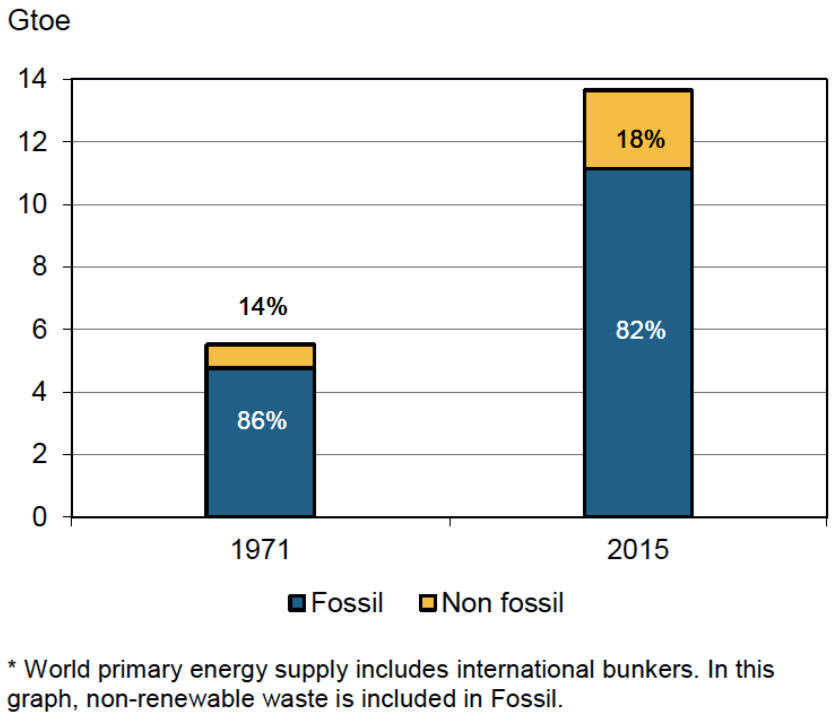

Figure 1-2: Comparison of the world primary energy supply [3]

1.1 Oxygen-fired Pressurized Fluidized Bed Combustion

Without doubt the predominant energy supply must be switched to renewable sources, however the immediate energy demand is likely to be met by conventional fossil fuel combustion until the alternative energy sources are able to reliably produce significant amount of energy. Coal has proved to be stable in both supply and price and thus it is likely to play a significant role in energy generation in foreseeable future [4]. Clean coal combustion technology with downstream carbon dioxide capture and sequestration is thereby considered a promising approach in GHG emission reduction. Clean coal combustion allows emitted CO_2 to be captured directly from the process in high purity and being ready for sequestration. Oxygen-fired combustion uses nearly pure O_2 instead of air in fossil fuel combustion. Thus, separation of CO_2 from N_2 in the combustor flue gas, which now predominantly contains CO_2 and condensable water, is avoided (Figure 1-3). Because of N_2 elimination, concentration of CO_2 in flue gas could reach 90%-98% [5], whereas the flue gas

from an air-fired coal combustor contains only 15% of CO_2 by volume [6,7]. Such unique feature results in cost reduction of both capital and energy cost comparing to other carbon capture technologies [8]. In addition, small efforts would be required in retrofitting existing facilities since oxygen-fired combustion shares the similar combustion principles as the conventional air-blown combustion.

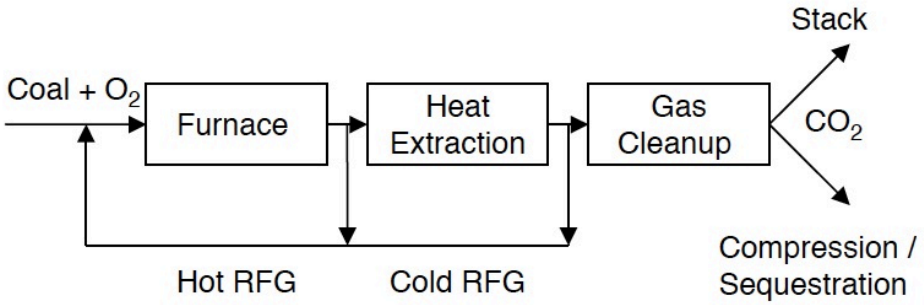

Figure 1-3: General process flow diagram of an oxy-fuel coal combustion. Here RFG is Recycled Flue Gas.

An advanced technology for oxy-fuel coal combustion is an oxygen-fired pressurized fluidized bed combustor (Oxy-PFBC) [9]. According to Fassbender [10] and Zheng et al. [11], a pressurized combustor can achieve a gain in net energy efficiency which results in a reduction in capital cost and electricity cost compared to atmospheric combustion. Hong et al. [12] proved that a rise in net power efficiency (HHV) from 30.2% to 33.5% could be achieved as pressure went up to 1000 kPa. However, there existed an optimal pressure above which the net power efficiency would not be affected, which was claimed to be 1000 kPa according to Hong et al. [12]. Moreover, Heitmeir et al. [13] reported that pressure also provides a positive effect on combustion efficiency. Finally, according to Yang et al [14], with the increase in pressure the minimum fluidization velocity of the large bed particles would decrease resulting in a reduction of erosion due to lower gas velocity, especially for heat exchange surfaces housed inside the bed. An example of a process which

includes Oxy-PFBC technology has been developed by the Gas Technology Institute-GTI (USA) as shown in Figure 1-4.

To evaluate the performance of an Oxy-PFBC technology, a $1MW_{th}$ pilot plant was built and is currently under operation at NRCan CanmetENERGY (Ottawa, Ontario, Canada) in collaboration with GTI [15]. The combustor uses a bimodal particle mixture where large bed particles (e.g. dolomite or sand of ~ 1 mm) are fluidized along with pulverized fuel particles with mean diameters ranging from 70 to 100 µm. With an in-bed heat exchanger for achieving a greater heat transfer rates per unit surface, there has been a need for the bed-to-surface heat transfer to be studied at operating conditions specific to this facility.

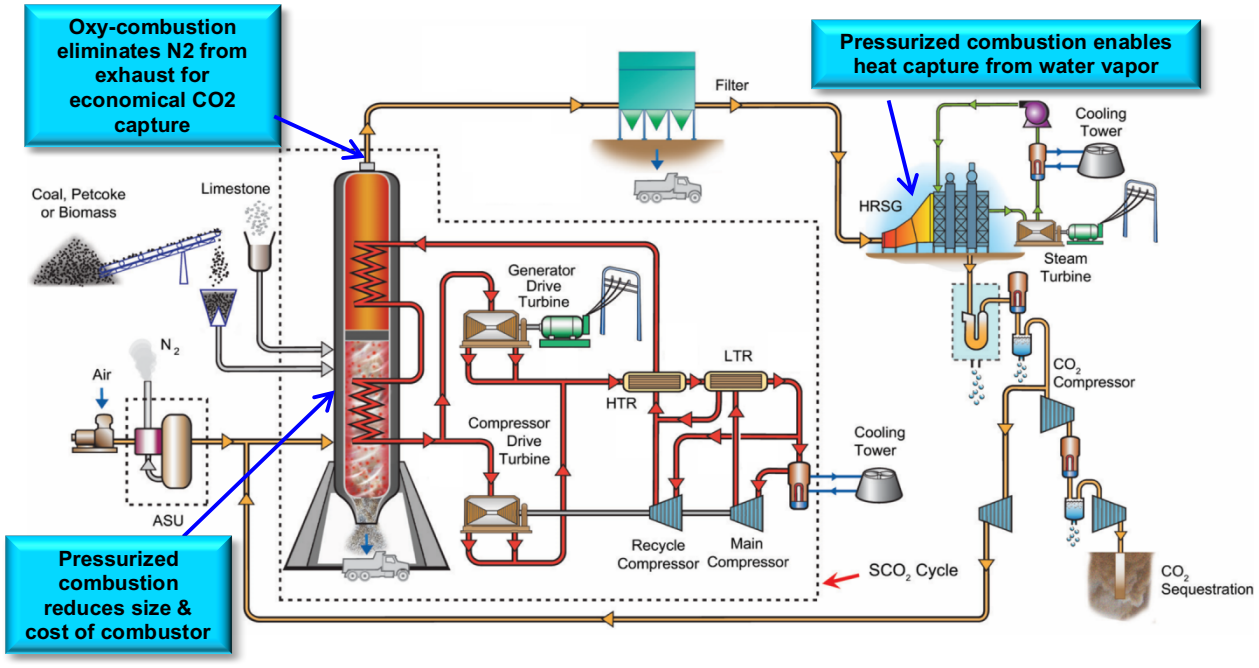

Figure 1-4: GTI zero emission Oxy-PFBC power plant concept vision [16]

1.2 Research Objectives

The knowledge of bed-to-surface heat transfer coefficient is a key parameter in designing in-bed heat exchangers in the Oxy-PFBC. The aim of this work was to determine the bed-to-surface heat transfer coefficient for a horizontal tube bundle immersed in a bed of large particles ($\overline{D_p} = 1$ mm) fluidized along with continuous injection of fine particles ($\overline{D_p} = 60$ μm) under cold flow operating conditions similar to those of the Oxy-PFBC located at NRCan CanmetENERGY. The specific objective of this research was to determine the effects of the following parameters on the bed-to-surface heat transfer coefficient:

- Fluidization pressure: 101, 600 and 1200 kPa
- Fluidization excess gas velocity (U_e): 0.21, 0.29 and 0.51 m/s
- Fine particles feed rate: 0, 9.5 and 14.5 kg/h
- Heating rod location within the horizontal tube bundle: 2nd row vs. 4th row

1.3 Thesis Outline

The thesis consists of 4 chapters. Chapter 1 introduces the background information in relation to this research. Chapter 2 presents a literature review of bed hydrodynamics as well as the bed-to-surface heat transfer in gas-solid fluidized beds. Chapter 3 is an in-preparation journal manuscript summarizing the results of this research. The manuscript entitled "heat transfer in pressurized fluidized bed with addition of fines" will be submitted to the journal Powder Technology. This chapter provides details on the experimental apparatus used as well as results obtained for the bed–to-surface heat transfer coefficient in the presence of an immersed horizontal tube bundle while fluidizing a bimodal particle mixture at various operating conditions. Chapter 4 provides a summary of conclusions obtained and suggestions for the future work.

References

[1] P.D. Jones, K.E. Trenberth, P. Ambenje, R. Bojariu, D. Easterling, T. Klein, D. Parker, J. Renwick, M. Rusticucci, B. Soden, Observations: surface and atmospheric climate change, Climate Change, (2007) 235–336.

[2] NASA, NASA: Climate Change and Global Warming, https://climate.nasa.gov/.

[3] IEA, CO_2 Emissions from Fuel Combustion 2017, OECD Publishing, (2017).

[4] S. Ansolabehere, The future of coal, (2006).

[5] Z. Nie, Life cycle modelling of CO_2 capture and storage in energy production, Department of Earth Science and Engineering, Imperial College London, (2009).

[6] I.T.C. on C.U. and F. Systems, A.S. of M.E.F. and C.T. Division, C.T. Association, U.S.D. of Energy, Proc. 30th Int. Tech. Conf. Coal Util. Fuel Sys., (2005).

[7] I. Ghg, Improvement in power generation with post-combustion capture of CO_2, Cheltenham Int. Energy Agency Greenh. Gas R&D Program. (2004).

[8] B.J.P. Buhre, L.K. Elliott, C.D. Sheng, R.P. Gupta, T.F. Wall, Oxy-fuel combustion technology for coal-fired power generation, Prog. Energy Combust. Sci. 31 (2005) 283–307.

[9] J. Andries, J.G.M. Becht, P.D.J. Hoppesteyn, Pressurized fluidized bed combustion and gasification of coal using flue gas recirculation and oxygen injection, Energy Convers. Manag. 38 (1997) S117–S122.

[10] A. Fassbender, Pressurized oxy-fuel combustion for multi-pollutant capture, 30th Int. Tech. Conf. Coal Util. Fuel Syst, (2005).

[11] C. Zheng, L. Zheng, R. Pomalis, R. Turner, B. Clements, Conceptual design and experimental study overview: flue gas treatment and CO_2 recovery experimental system for high pressure oxygen fired coal combustion, 33rd Int. Tech. Conf. Coal Util. Fuel Syst, (2008).

[12] J. Hong, G. Chaudhry, J.G. Brisson, R. Field, M. Gazzino, A.F. Ghoniem, Analysis of oxy-fuel combustion power cycle utilizing a pressurized coal combustor, Energy. 34 (2009) 1332–1340.

[13] F. Heitmeir, W. Sanz, E. Göttlich, H. Jericha, The Graz cycle–a zero emission power plant of highest efficiency, XXXV Kraftwerkstechnisches Kolloquium, (2003).

[14] W.-C. Yang, M. Dekker, Handbook of fluidization and fluid-particle systems, CRC press, (2003).

[15] S.A.Y. W. Follett, M. A. Fitzsimmons, S. V. Pisupati, C. G. Sonwane, S. Jovanovic, T. W. Manley, D. Hiraoka, Development of a pilot scale coal coal powered oxy-fired pressurized fluidized bed combustor wity CO_2 capture, Power-Gen Eur. Conf., (2015).

[16] W. Follet, M. A. Fitzsimmons, Enabling Technologies for Oxy-fired Pressurized Fluidized Bed Combustor Developmetn, Gas Technology Institute, (2015). https://www.netl.doe.gov/File%20Library/Research/Coal/Combustion/FE0025160-Enabling-Tech-for-Oxy-PFBC-Kickoff.pdf

Chapter 2 Literature Review

This chapter presents literature on two fundamental topics: gas-solid fluidization; and heat transfer in gas-solid fluidized beds. The literature on gas-solid fluidization consists 4 of parts: fluidization flow regimes and particle classification; gas bubble characteristics; particle elutriation; and the effect of tube bundle on bed hydrodynamics. The literature on heat transfer in gas-solid fluidized beds is mainly focused on bed-to-surface heat transfer mechanism as well as parameters that affect it such as pressure, gas velocity, particle size and heater location within a horizontal tube bundle. Correlations for estimating the overall convective heat transfer coefficient and the radiative heat transfer coefficient are also presented.

2.1 Gas-Solid Fluidization

When a gas passes through a bed of solids at a certain velocity the particles are supported by the drag force exerted by the gas and beyond this velocity solids start moving around. This is said to be the onset of fluidization, or minimum fluidization. The minimum fluidization gas velocity, which is denoted as U_{mf}, could be experimentally determined by measuring pressure drop across the bed at various superficial gas velocities [1]. And it could also be estimated by correlations proposed by many researchers [1–3].

Above minimum fluidization, various fluidization flow regimes are developed as gas velocity increases (Figure 2-1). Beyond minimum fluidization, bubbling flow regime is achieved where small size gas bubbles, usually smaller than 40% of bed diameter [4], form at the distributor plate and rise to the bed surface. As the gas velocity is further increased, the gas bubble diameter increases until the bubble diameter reaches 40% of bed diameter. Turbulent fluidization will be

achieved by continuing increasing the gas velocity, where small gas voids and particle clusters dart to and fro and the bed surface becomes undistinguishable. Further increase in gas velocity will eventually lead to the bed particles entrainment from the top of the column and then recycled back to the bottom of the bed through a cyclone. This flow regime is called fast fluidization. If particles are not captured and recycled back to the bed, then the flow regime is called pneumatic conveying.

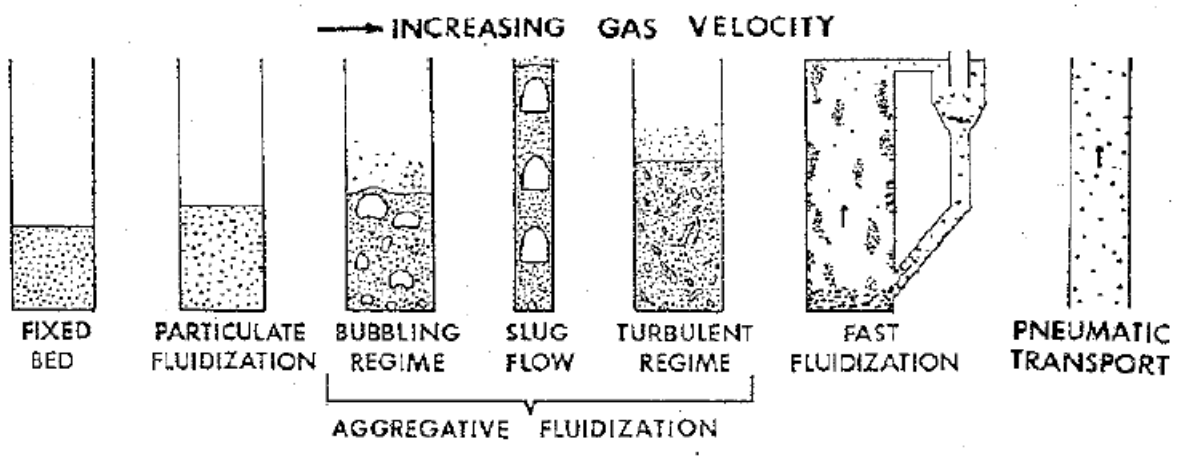

Figure 2-1: Fluidization flow regimes [1].

Particles property is another foundation for knowing the fluidization behavior without a doubt. A useful classification scheme was developed by Geldart [5] which categorized particles into 4 groups according to their characteristic fluidization behaviors, depending on particle mean diameter and relative density between solid particles and fluidization fluid (Figure 2-2).

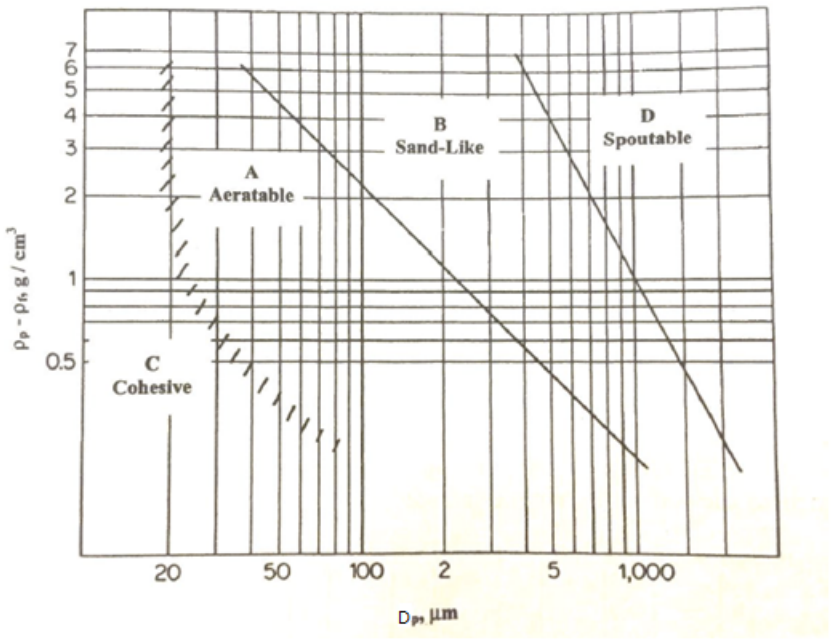

Figure 2-2: Particle classification proposed by Geldart [5]

Group C particles refer to those that are very fine and usually prone to electrostatic effects and inter-particle forces, which result in severe gas channeling and difficulties to be fluidized, thus being categorized as a cohesive group [4,5]. Group A particles are fluidized as particulate fluidization at minimum fluidization gas velocity, experiencing a homogeneous bed expansion, and gas bubbles appear as gas velocity reaches minimum bubbling velocity [4]. Group B particle are widely studied with the immediate appearance of bubbles at minimum fluidization gas velocity [4], and are applied to a wide range of particle sizes, 100 – 1000 µm. Similar to Group B particles, immediate bubbling regime is achieved at minimum fluidization with larger particle sizes known as Group D particle. However more rapid coalesce of bubbles are observed with such particles and hence they spout readily [4].

2.1.1 Gas Bubble Characteristics

Gas bubble size is one key characteristic that governs the bed hydrodynamics. Efforts [6–9] have been made in measuring bubble size including the usage of intrusive and non-intrusive techniques. A common intrusive technique is an optical fibre probe that is typically applied to measure local voidage inside fluidized beds. Bai et al. [6] measured bubble passage time during its rising through the tip of the optical probe and thus obtained the estimated bubble size based on the bubble rise velocity model of David-Harrison [10]. Non-intrusive measurements refer to those that are based on X-ray and capacitance tomography [11,12], and most commonly, the pressure fluctuation analysis [8,9,13]. By using the differential pressure signal, measured by a differential pressure sensor, Bi [8] was able to develop a method for estimating bubble size. Liu et al. [9] also proposed a correlation for estimation of bubble diameter ($d_{B,\Delta P}$) based on the differential pressure fluctuation analysis [8,13].

$$d_{B,\Delta P} \propto \frac{\sigma_{\Delta P}}{\rho_p g\left(1-\varepsilon_{mf}\right)} \tag{2-1}$$

where $\sigma_{\Delta P}$ is the standard deviation of bed differential pressure, ρ_p is the particle density, and $\varepsilon_{mf}$is the bed voidage at minimum fluidization.

2.1.2 Particle Elutriation

Particle elutriation characterizes the selective removal of particles of individual size from the fluidized bed [4]. As the fluidizing gas velocity exceeds the particles terminal velocity (U_t), the particles will be entrained from the fluidized bed [14,15]. Those with larger particle sizes and densities and hence having a higher terminal velocity than the gas velocity will remain in the bed. The terminal velocity of a single spherical particle is given in equation (2-2) [16,17],

$$U_t = \sqrt{\frac{4D_p(\rho_p - \rho_f)g}{3\rho_f C_D}} \tag{2-2}$$

where ρ_f is the gas density, and C_D is the drag coefficient.

As show in in equation (2-3), Turton and Levenspiel [19] developed a correlation for drag coefficient applicable to the entire range of particle Reynold`s number, Re_p.

$$C_D = \frac{24}{Re_p}\left[1 + 0.173(Re_p)^{0.657}\right] + \frac{0.413}{1 + 16.300(Re_p)^{-1.09}} \tag{2-3}$$

The process of particle elutriation [4] starts from that particles are first being transferred from the bed to the freeboard with their initial velocity. Carried out with the upward gas, rising particles will then adjust their velocity to the inferior gas velocity. Finally, particles will be transferred to the gas outlet. For the first sub-process of particle elutriation, gas bubble eruption at surface of bed was considered as the mechanism of particle transportation from bed to freeboard. Particle ejection from a bubble bursting at the surface of bed consist of two major mechanisms. One is that particles ejecting from the nose of gas bubbles, as shown in Figure 2-3a, which is being considered as the governing mechanism by Zenz et al. [14] and Chen et al. [20]. The second mechanism, being considered as the governing mechanism by George et al. [21], is the particles ejecting from the wake of a bubble, as shown in Figure 2-3b. Pemberton et al. [22] claimed that both mechanisms governed in their measurements while particles were ejected from the roof of coalescing bubbles bursting at the surface of bed as well as from their wake to freeboard (Figure 2-3c). Pemberton et al. [22] also claimed that for Group A particles with high velocities the roof ejection mechanism predominates whereas the wake ejection mechanism predominates for Group B particles with lower velocities.

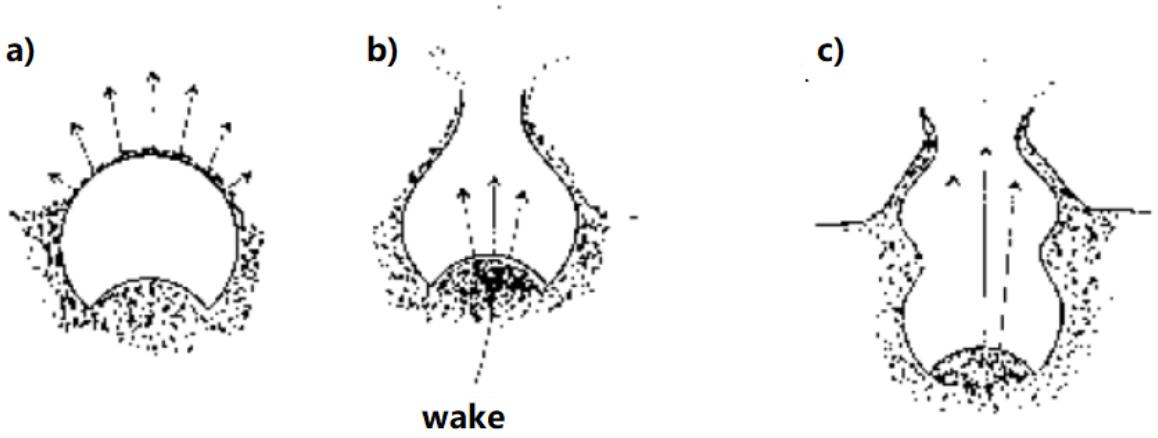

Figure 2-3: A gas bubble bursting at the bed surface and ejecting solids into the freeboard from (a) its roof, (b) its wake, and (c) the wake of two coalescing bubbles [4].

The initial velocity of particles carried out by bubbles bursting at the bed surface was found to be significantly higher than bubble rise velocity [21,23]. Researchers [21,24] also found that the starting velocity of particles being ejected into freeboard could be as twice as bubble rise velocity. After being ejected into freeboard, particles with certain velocities will decelerate and either fall back to the bed or are being transported to the gas outlet by up-flowing gas [4]. Beside the particle movement profile in freeboard, there is also temporary fluctuations caused by bubble bursting at the bed surface [4].

2.1.3 Effect of an in-bed Tube Bundle on Bed Hydrodynamics

Internal tubes immersed in the bed will certainly affect bed hydrodynamics. Rowe et al. [25] revealed such phenomenon using X-ray photography and found that horizontal tubes were able to generate bubbles at gas velocity exceeded the minimum fluidization velocity (Figure 2-4). It is found that with presence of in-bed staggered horizontal tubes, bubbles brake up contacting bottom-row of the tube bundle and then coalesce immediately at one row above [25–27]. Grace [1] stated that horizontally positioned tubes could induce local fluidization as well as formation of bubbles

at side of the tube at a superficial gas velocity smaller than the minimum fluidization velocity. Same phenomenon was concluded by Catipovic [28].

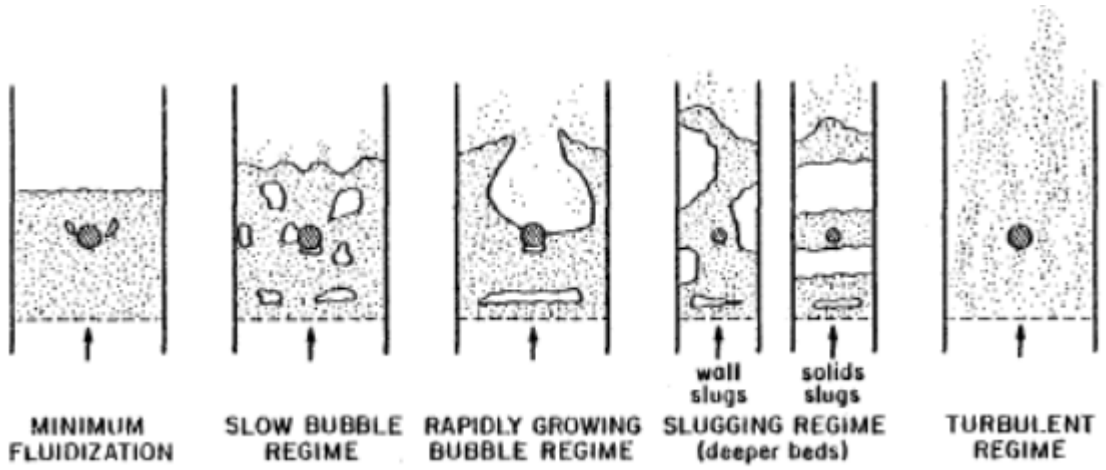

Figure 2-4: Presence of a single in-bed tube at various fluidization flow regimes [28]

According to Glass et al. [29], at a gas velocity in excess of minimum fluidization velocity, a gas film would form at the bottom of a tube while bubbles detaching from its sides and a defluidized zone forming at the top of the tube (Figure 2-5). Bubbles forming at the sides of the tube follow an alternative pattern where one forms at one side and then another at the opposite side, and hence particles are periodically swept at the side of the tube [1]. And with the impinging of bubbles to the tubes, particles in the defluidized zone at the top of tube will be replaced. Recombination of broken bubbles could be impeded by upper tubes and thus resulte in a significant reduction in mean diameter of gas bubbles [1].

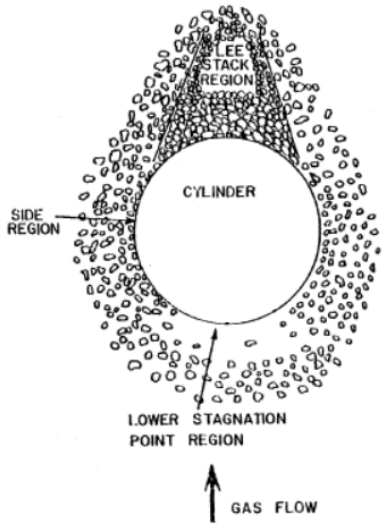

Figure 2-5: Void distribution around an in-bed tube [28].

Moreover, Wiman et al. [30] and Olsson et al. [31] investigated the effect of different arrangements of tube arrays on bed hydrodynamics for both fine and coarse particles in a pressurized fluidized bed. Conclusions were drawn that a more uniform radial flow pattern would be achieved with the presence of a tube bank [31], and a denser tube bank would trigger such transition under a lower gas velocity and pressure combination [30]. Wiman et al. [30] also stated that despite of the common feature of large bubble formation prevention shared by a sparse ($S_H \times S_V = 60 \times 52\ mm$) and a dense ($S_H \times S_V = 42.5 \times 50\ mm$) tube bundle, a dense arrangement makes a stronger constraint over particle motion and creates more local voidage around the tube. Wiman et al. [30] also argued that horizontal pitch in between tubes are privileged over vertical pitch on affecting bed behavior. In general, where the effect on bubble hydrodynamics being enhanced by arrays of tubes, minor effect was performed on bubble size distribution due to a single tube. Grace [1] also argued that the most effective tube arrangements is when tubes are being positioned at 45° with a centre to centre pitch of 2-2.5 times of the tube diameter.

2.2 Heat Transfer in Gas-Solid Fluidized Beds

Heat transfer in a gas-solid fluidized bed could consists of three mechanisms, namely gas-to-particle, particle–to-particle, and bed–to-surface heat transfer. Gas-to-particle heat transfer happens as cold gas flows through the bed and being heated up by particles of higher temperatures. However, researchers found that gas temperature rises quite fast as the temperature difference between gas and particles decreased by a hundred of times only a short distance above the distributor plate (i.e., 5-10 particle diameters) due to an intensive heat transfer between gas and particles which results from a large interfacial area [32,33]. Since bed heights are commonly ranging from 0.5-1 m in industrial processes, it could be safely addressed that temperature is equal across the bed height [34] and thus gas-particle mixture is considered isothermal in many designs [4].

Particle–to-particle heat transfer is considered to be important when particles of different temperatures are mixed together. Wen et al. [35] also indicated that particle-to-particle heat transfer through points of contact was negligible.

As for bed-to-surface heat transfer, Oka et al. [34] stated that around 30%-50% of total generated heat in solid fuel fluidized bed combustion was transferred to internal heat transfer surfaces which were in contact with the fluidized bed and thus bed-to-surface heat transfer could be considered as the most important heat transfer mechanism in fluidized bed combustors. The bed-to-surface heat transfer basically consist of three superimposed components: convective (h_{conv}), conductive (h_{cond}) and radiative (h_r) terms [1,39,36]. The convective term refers to the heat transfer performed by gas flowing within gas bubbles or in emulsion phases while contacting with internal heat transfer surfaces. The conductive term refers to the mobile particle/particle packets conducting heat while in contact with the heat transfer surface. Finally the radiative term comes from radiant heat transfer.

A common case for bed-to-surface heat transfer is that convective (h_{conv}) and conductive (h_{cond}) terms are group together as an overall convective heat transfer term (h_C) [37-39]. Thus, the bed-to-surface heat transfer, as shown in equation (2-3), could be presented as the summation of gas convection heat transfer during gas bubble contact, particle conduction heat transfer during particle contact, and radiation heat transfer [4].

$$h_W = h_{conv} + h_{cond} + h_r = h_C + h_r = f_l h_l + (1 - f_l) h_d + h_r \quad (2\text{-}3)$$

where h_W is bed-to-surface heat transfer coefficient, f_l is the time fraction of lean phase contacting the heat exchange surface, h_l is the heat transfer coefficient of the lean phase contacting the heat exchange surface, h_d is the heat transfer coefficient of the dense phase contacting the heat exchange surface.

The convective heat transfer term is found to be dominant for large-sized particles (Geldart Group D) [1,40,41] whereas the conductive heat transfer term to be predominated for small particles (Geldart Group A, B, C) [40,42,43]. The radiation heat transfer is found to be significant with bed temperatures above 600°C [34].

2.2.1 Heat Transfer Measurement Techniques in Gas-solid Fluid Beds

Despite the fact that the heat is being transferred from the bed to a heat exchange surface in real systems such as fluidized bed combustors, in cold flow studies, the heat transfer is measured from a heated surface to the bed. Thus, a heating rod which could be heated up to a certain temperature by an external power supply it typically used to provide heat to the fluidized bed. Therefore, heat transfer coefficient (h_W) is determined by using equation (2-4):

$$h_W = \frac{IV}{A(T_t - T_b)} \tag{2-4}$$

where A is the surface area of the heating rod, I is current, V is Voltage, T_t is temperature around the tube surface, and T_b is the bed temperature.

The most common way as shown in Figure 2-6, which is also employed in this research, is using a heating cartridge placed inside a sleeve made of copper [43, 52, 54, 55, 57] or wood [53]. The heating cartridge could be a calrod [43, 52, 54, 57, 70], a winding heating coil on a stainless-steel tube [55] or a glass fiber covered with nichrome ribbon which could be electronically heated [53]. To measure the bed as well as the heated surface temperature, thermocouples are commonly placed on and around the heating surface [43, 52-55, 57, 70].

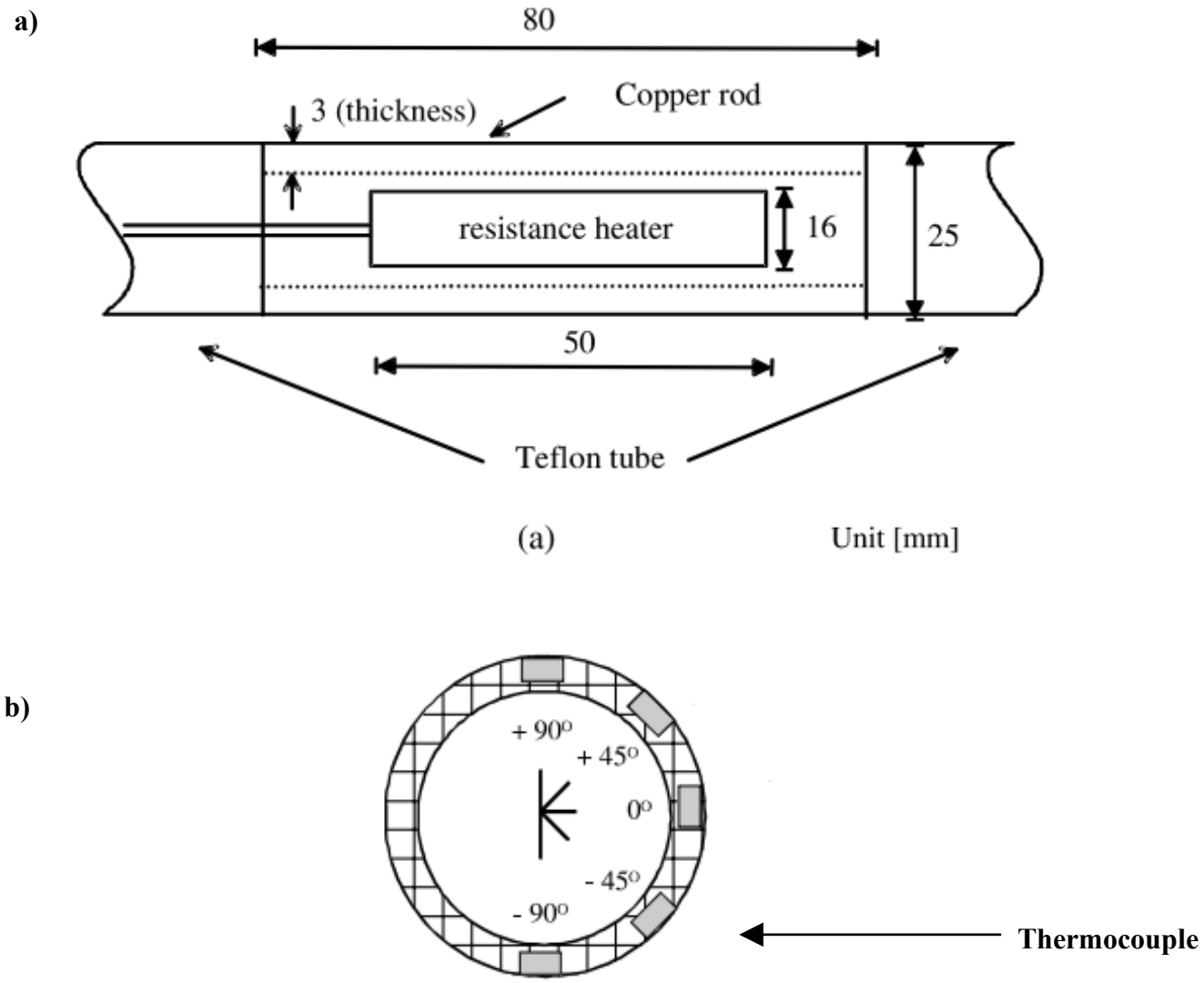

Figure 2-6. Heating rod a) assembled by copper rod with resistant heater inside; b) thermocouples placed around the tube surface [70].

Borodulya [47] used a heat transfer probe with a single winding of 70 μm diameter copper wire glued around its surface. The probe was calibrated at 323.2 K which being treated as a resistance thermometer in arm of a Wheatstone bridge and thus the heat transfer coefficient could be obtained according to the power supplied for restoring the bridge balance at various fluidizing conditions.

Instead of using a heating cartridge, Chandran [57] used a 31.75 mm diameter of solid Lexan rod bonding with eight strips of 50.8 μm thick Inconel foil was used as the heat transfer probe. Each strip of Inconel foil was heated by an individually controlled AC power supply and the power was adjusted to obtain a uniform temperature distribution around circumference of the tube. Miniature thermocouples were placed underneath the foil strips at 45° intervals around the tube and collected temperature were corrected to obtain surface temperature at the top of the heated foil strips.

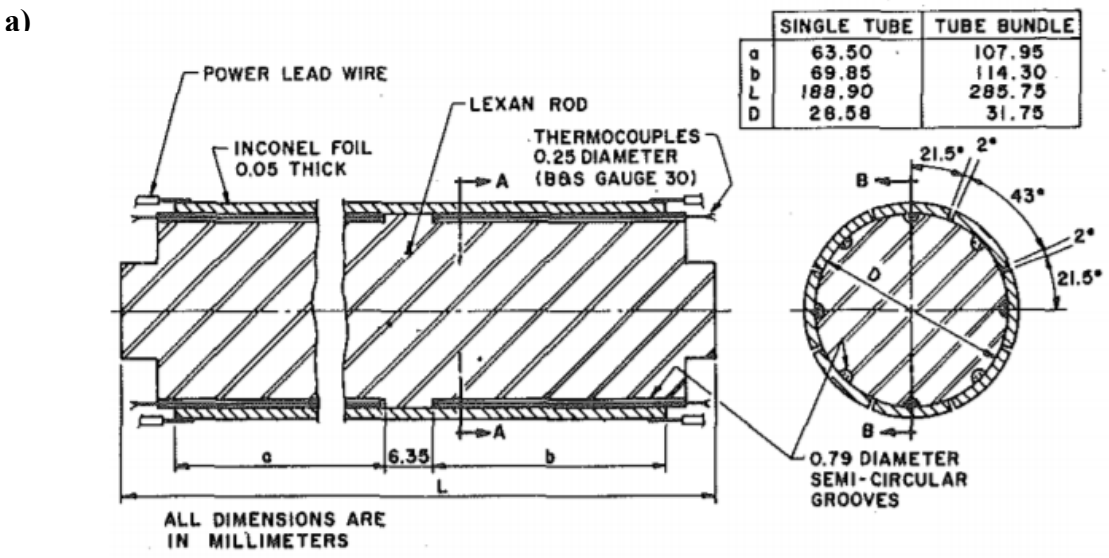

Figure 2-7.The schematic of heat transfer test section [57].

2.2.2 Effect of Pressure on Heat Transfer

Effect of fluidization pressure on bed-to-surface heat transfer was first studied by Traber et al. [44] for a range of 0.1 to 23 MPa where they claimed that the bed-to-surface heat transfer increased with increasing pressure. Then Rabinovich et al. [45] and Borodulya et al. [46] confirmed the same conclusion. Rabinovich et al [45] suggested that the increase in bed-to-surface heat transfer might result from a more uniform fluidization as the gas is better distributed within the bed.

Botterill et al. [40] then investigated the overall convective heat transfer coefficient (h_C) at ambient temperature in a 0.114 m diameter fluidized bed of copper shots (150 and 625 μm), sands (160,

800 and 2740 μm) and coal (1430 μm) under various pressures (0.1 and 1.13 MPa). In their case the fluidized bed housed an internal vertical heat transfer surface. For copper shot of 150 μm diameter, bed-to-surface heat transfer coefficient at 1000 kPa was roughly 15% higher than that at atmospheric pressure (Figure 2-8) whereas for 625 μm diameter copper shots the maximum bed-to-surface heat transfer was nearly doubled as pressure increased from atmospheric to 1000 kPa (Figure 2-8). Moreover, for large particles, bubbling behavior became more regular and minimum fluidization velocity reduced more comparing to small particles. They concluded that the overall convective heat transfer coefficient was barely dependent on pressure for small particles whereas it increased along with the rise in pressure for large particles.

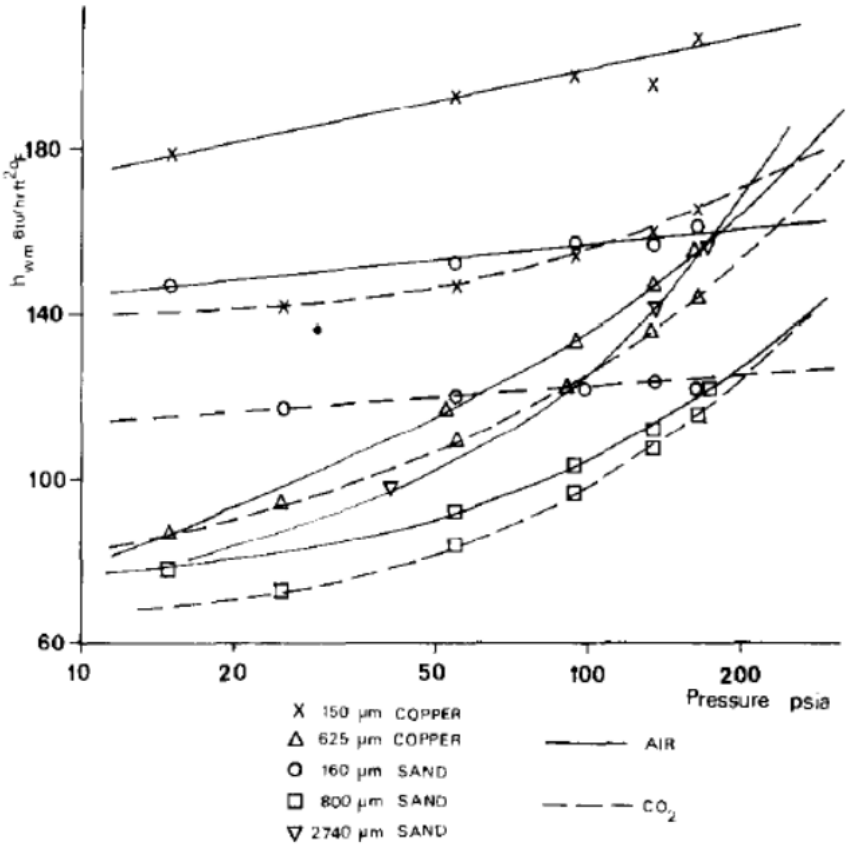

Figure 2-8: Variation in maximum bed-to-surface heat transfer coefficients at different pressures for various particle sizes [40].

Later, Denloye et al. [43] also studied overall convective heat transfer coefficient, using a 0.114 m in diameter cylindrical column with a 0.380 mm static bed of copper shot (160, 340, and 620 μm), sand (160, 590, 1020, and 2370 μm) and soda glass (415 μm) fluidized by various gases (air, argon, carbon dioxide and freon) under operating pressures ranging from 0.1 to 1 MPa. Gas temperature was kept constant at the inlet of the fluidization column. They stated that the increase in maximum overall convective heat transfer coefficient along with increasing pressure was mainly accounted by the increase in gas convection, which resulted from the increase in gas heat capacity.

In 1984, Borodulya et al. [47] studied the bed-to-surface heat transfer for large particles fluidized in presence of a horizontal in-bed tube bundles. They used a 0.1 m in diameter cylindrical stainless-steel column containing a bed with a 0.1 m static height. They tested three tube bundles consisting of inline square arranged 0.013 m diameter wood cylinders. Each of the bundles consisted of 25, 9 and 5 of cylinders with 0.0105, 0.0293 and 0.0390 m center-to-center spacing pitches respectively. Four types of particles were used as bed material including glass beads (mean diameters of 3.1 mm and 1.25 mm), sand (mean diameters of 1.225 mm 0.794 mm). Air was used as fluidization gas and operating pressures were set at 1.1, 2.6, 4.1 and 8.1 MPa. They confirmed that the bed-to-surface heat transfer coefficient at higher pressure was consistently larger than those at lower pressure across all conditions. They also concluded that high pressure condition resulted in smooth fluidization. It was explained that a rise in gas density would prevent not only the formation of particle bridging in between two tubes, but also the Lee stack region at the top of tube or any stagnant solids around the tube. In general, increasing pressure would change bed hydrodynamics [47,48] as well as the gas density [47] and thermal conductivity [48], and hence resulting in an increase in the bed-to-surface heat transfer.

2.2.3 Effect of Gas Velocity on Heat Transfer

Gas velocity as one of variables affecting bed-to-surface heat transfer is most studied for decades [40,43,49-51] where an increase in heat transfer coefficient along with the increase in gas velocity is observed. Botterill et al. [40] reported that for a fluidized bed (0.0114 m in diameter) housing a vertical heat transfer surface there was a sharp rise in bed-to-surface heat transfer coefficient at a gas velocity 1.1 times minimum fluidization velocity. Then a rapid drop in heat transfer coefficient occurred with further increase of gas velocity (Figure 2-9). They accounted the reduction in heat transfer, after reaching a maximum, to the transition of fluidization regime to aggregative fluidization since forming slugs detrimentally decreased particle packing density.

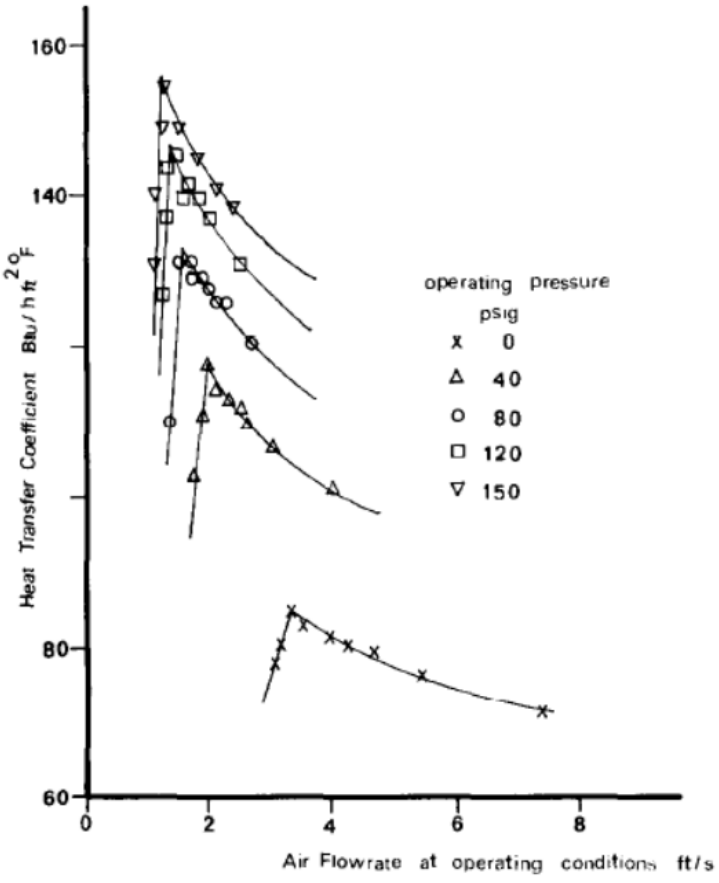

Figure 2-9: Variation in heat transfer coefficient of an air-fluidized bed of 625 μm copper shots as a function of gas velocity and pressure [40]

Denloye et al. [43] reported that for various size of particles, the heat transfer from a heating surface to the bed increased with increasing gas velocity until a maximum was reached and the optimum gas velocity was approximately 30% greater than the minimum fluidization velocity. Moreover, it was reported that there were two distinct maximum heat transfer coefficients observed for large particles with increasing gas velocity (Figure 2-10). They explained that the first peak resulted from the simultaneous increase of bed mobility and bed expansion, where bed mobility positively affected heat transfer while bed expansion did other way around. After the first peak, the further increase of heat transfer coefficient was accounted by the greater particle circulation rate inside the bed due to formation of large slugs. However, Botterill et al. [40] also concluded that there were no such two distinct peaks in bed–to-surface heat transfer for fine particles (referring to 150 μm copper shots in their experiment). For fine particles, slugging had no effect on particle circulation and as gas velocity was increased beyond the optimum velocity, increasing bed expansion consistently decreased the bed-to-surface heat transfer.

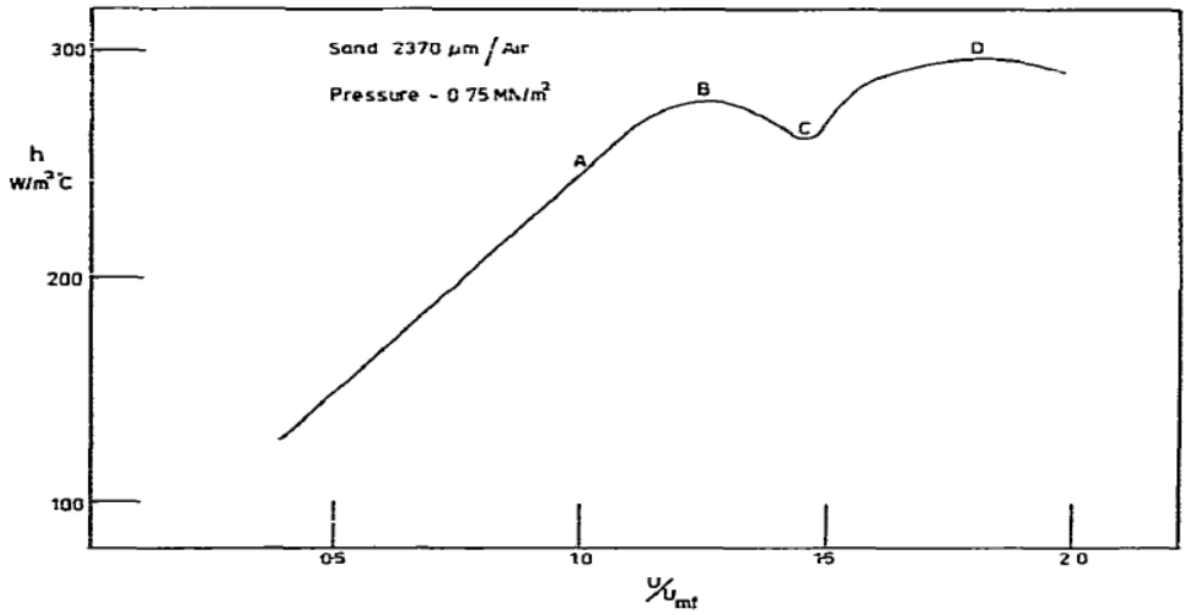

Figure 2-10: Variation in bed-to-surface heat transfer coefficient with fluidization rate for a sand /air system [43]

Grewal et al. [52] used a square fluidization column ($30.5\times30.5\,cm$) with a horizontally positioned cylindrical heating tube placed 0.213 m above the distributor plate. Various types of particles (silicon carbide, alumina, silica, dolomite, glass beads, and lead glass) were used as bed material with mean diameter ranging from 167 to 504 μm. Two pressure probes were located above and below the heating rod, thus the pressure drop across the bed could be measured. They reported the same trend as previous studies where the bed-to-surface heat transfer increased with increasing gas velocity until a maximum was achieved and then a reduction occurred. A further explanation other than that by Botterill et al. [40] was given that the maximum heat transfer was attained because of low particle residence time at the heat transfer surface and large particle concentration close to the heating surface. The increase in gas velocity led to better stirring action of bubbles, or bubble frequency, which resulted in a better solids mixing. Particle residence time at the heat transfer surface decreased with the increase of solids mixing and thus positively affected the heat transfer. On the other hand, the particle concentration close to heat transfer surface was decreased

with the increase of gas velocity which would led to a reduction in the heat transfer rate. In general, the bed-to-surface heat transfer at a specific fluidizing gas velocity was dependent on the net contribution of the two opposite factors.

2.2.4 Single Tube vs. Tube Bundle

As mentioned in section 2.1, the bed hydrodynamics would be affected by an in-bed tube bundle which would eventually lead to different heat transfer behaviors comparing to a single in-bed tube. Einshtein et al. [53] studied the local heat transfer coefficients of a horizontal tube immersed in a rectangular fluidized bed ($0.38\times0.38\,m$) where the tube was positioned 0.435 m above the distributor plate. The static bed height was 0.5 m with quartz sand particles of 350 μm in mean diameter. They reported that the maximum heat transfer happened at the side of the tube and it would increase along with the rise of gas velocity. With the increase in gas velocity, the local heat transfer coefficient at upstream side of the tube was sharply increased and the gradient was greater than those at lateral zone of the tube. The rise of heat transfer coefficient could be accounted by the increase in the intensity of motion of solid particles close to the heat transfer surface [53]. However, with a greater effect of gas bubbles contacting the side of the tube, the positive effect due to solid particle motion was somewhat counteracted. The heat transfer coefficient downstream of the tube was reported to increase with the increase in gas velocity due to the increase in mobility of solid particles at the defluidized cap above the tubes.

In 1979, Saxena et al. [54] studied heat transfer using various types of immersed horizontal tubes (a single tube, an in-line tube bundle and a staggered tube bundle) placed in a square column ($30.5\times30.5\,cm$). Silica sand with two sizes (mean diameters of 167 μm and 504 μm) were used as the bed material. For the in-line tube bundle, the vertical and horizontal pitches were set as 4 times the column diameter (D_T) whereas they were set to 2 D_T and 4 D_T for staggered tube bundles

respectively. With both sizes of silica sand, they reported that the bed-to-surface heat transfer would not change as long as vertical and horizontal pitches were greater than 2 D_T and 4 D_T respectively for the staggered tube bundle or both of which were greater than 4 D_T for the in-line tube bundle.

Zabrosky et al. [55] used large particles in studying the effect of a horizontal tube bundle. A rectangular column ($40 \times 24\ cm$) with a Plexiglas front wall allowing visual observation was used as the fluidization column. The in-bed tube bundle contained 5 to 7 rows of 0.030 m diameter horizontal tubes. The bottom row of tubes was located 0.15 m above the distributor plate. In-line and staggered tube arrangements were used with various spacing. There were 5 sets of tube spacing arrangements for the in-line tube bundle ($S_H \times S_V = 100\times100\ mm; 100\times50\ mm; 80\times80\ mm;\ 60\times60\ mm; 45\times45\ mm)\ and$ 3 sets for the staggered tube bundle ($S_H \times S_V = 100\times100\ mm; 60\times60\ mm; 45\times45\ mm$). Two types of particles were used as bed material, spherical millet seeds with mean diameter of 2 mm and non-spherical crushed fire clay with mean diameter of 3 mm. The static bed height varied from 0.270 m to 0.420 m where tube bundles were fully immersed in bed across all tube arrangements. Zabrodsky et al. [55] reported that the bed-to-surface heat transfer coefficient of a single horizontal tube coincides with that of in-line tube bundles at $S_H = S_V > 2D_T$ and the heat transfer coefficient was consistently greater than the values for tube bundle with $S_H = S_V = 60\ mm$. They accounted such reduction in heat transfer coefficient on the possible "congestion" of closer tube arrangements. Moreover, a reduction in horizontal pitch could significantly reduce the bed-to-surface heat transfer coefficient since the horizontal pitch decreased from 100 mm to 50 mm while the vertical pitch remained the same as 100 mm. However, such reduction was not observed in the reverse case where the vertical pitch reduced from 100 mm to 50 mm while the horizontal pitch remained at 100 mm. It could be

explained that a closer arrangement of tubes in horizontal plane hampers solids mixing more appreciably than the decrease of tube spacing in a vertical plane. Zabrodsky et al. [55] also reported an unusual wavy behavior of heat transfer coefficient for fine clay bed, housing the $100\times50\ mm$ in-line tube bundle, as gas velocity was increased. They concluded that this could be attributed to particle bridging between adjacent tubes. Stable bridges were increasingly formed with the increase in the gas velocity and thus heat flux decreased because of stationary bridge abutments as well as over the tube surface area in contact with gas voids. Further increase of gas velocity would increase the bridge mobility and hence heat transfer should be enhanced.

As mentioned in section 2.2.2, Borodulya et al. [47] studied the bed-to-surface heat transfer coefficient at elevated pressures, using a cylindrical fluidized bed housing an in-line tube bundle with 13 mm diameter wood cylinders placed in square arrangement. They reported that no effects of tube spacing was observed at the tube pitch of 1.5 D_T at high pressure. As mentioned before, they had concluded that a rise in gas density would prevent not only the formation of particle bridging in between two tubes, but also the Lee stack region at the top of tube or any stagnant solids around the tube.

Doherty et al. [56] studied the effect of tube spacing on the dependence of two ranges of gas velocities at ambient temperature. A single tube, an in-line and a staggered tube bundle were used in beds of silica sand (mean diameter of 488 μm) and red silica sand (mean diameter of 777 μm). Two types of tubes, 28.6 mm in diameter brass tubes and 50.8 mm diameter aluminum tubes, were used. The relative pitch of the in-line and the staggered tube bundles for brass tubes were 2.66, 5.32 and 2.66 respectively. For aluminum tubes the relative pitches were 1.5, 3 and 1.5 respectively. They reported that at a lower gas velocity range, heat transfer coefficient in the presence of the tube bundle was found to be greater than that with a single tube and the greatest value of heat

transfer coefficient happened with the presence of staggered tube bundle. They explained the fact that few bubbles were induced in bed with the single tube at lower gas velocity range and thus resulted in a poor solids mixing whereas the tube bundle might capture some rising bubbles, forming gas pockets underneath the tubes. Then the gas pockets collapsed, and smaller bubbles formed which eventually led to a better solids mixing comparing to the single tube case. With the presence of a staggered tube bundle, an even better bubbling effect was achieved thus leading to the greatest heat transfer coefficient. For higher gas velocity range, the highest heat transfer coefficient happened with the presence of a single tube, while the in-line tube bundle had the lowest value of heat transfer coefficient. According to Doherty et al.[56], with the increase of gas velocity a much better solids mixing occurred with a single tube, whereas for the tube bundles the trapped air pockets expanded downward until a maximum size was reached and then collapsed for bubble generation. Gas bubbles traveled in channels between adjacent tubes in the in-line tube bundle whereas for staggered tube bundle, bubbles encountered tubes of upper row, causing a good mixing and thus reaching a greater heat transfer coefficient.

2.2.5 Effect of heating Surface Location

The influence of the location of the heating tube within a tube bundle was investigated by Chandran et al.[57]. They used a 0.305 m square open-loop fluidized bed and studied heat transfer coefficient for different tube positions at atmospheric pressure and various gas velocities. Bed temperatures were measured by four thermocouples located around the heat transfer tube at 90° intervals. The staggered tube bundle consisted of ten rows of tubes where the heat transfer probe was located in the midst of the first row and the third row respectively. Soda lime glass particles (650 μm in diameter) were used as bed material and the static bed height was remained as 0.47 m. For heat transfer probe located in the 1st row of tube bundle, the maxim local heat transfer coefficient

switched from side to top of tube by increasing the gas velocity, whereas the peak remained at the top of the tube for heat transfer probe located in the 2nd row. As for time averaged heat transfer coefficient, all three configurations performed similarly where bottom-row obtained the lowest value and the inner-row achieved the highest (Figure 2-11).

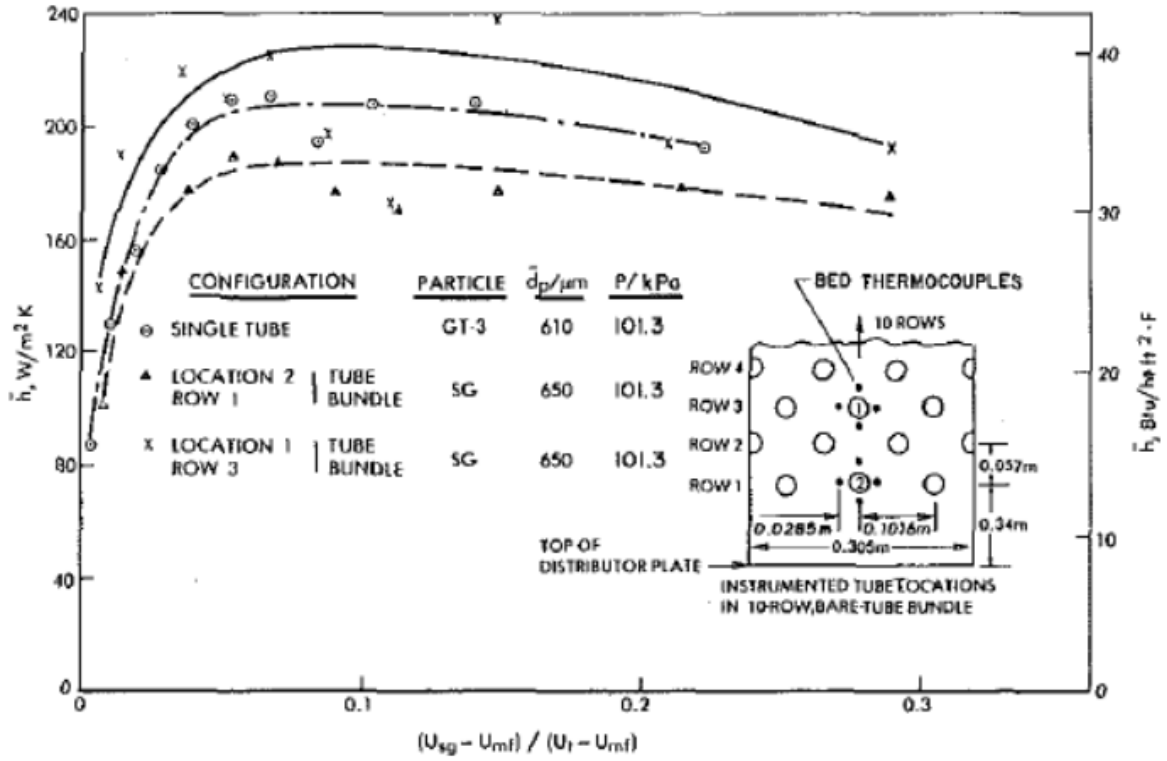

Figure 2-11: Comparison of average heat transfer coefficient around a single tube with those obtained around a tube at two locations within a tube bundle [57].

2.2.6 Effect of Particle Size on Heat Transfer

As mentioned in section 2.2, the dominant mechanism of overall convective heat transfer in gas-solid fluid beds is dependent on particle size. Particle classification proposed by Geldart [5] has been widely applied in heat transfer studies for immersed surfaces as it describes the bed hydrodynamics in gas-solid fluidized bed. On the other hand, Saxena et al. [49] proposed another approach on particle classification which considered both thermal and hydrodynamic properties.

According to Saxena et al. [49], particles were classified by 4 major groups named as group I ($3.55 < Ar < 21700$), IIA ($21700 < Ar < 130000$), IIB ($1.3\times10^5 < Ar < 1.6\times10^6$) and III($Ar > 1.6\times10^6$). For beds with large particles (Geldart group D or groups IIB and III), the gas convection predominates whereas for small particles (Geldart group A, B, C or group I and IIA) the particle conduction predominates. Efforts were made in studying the effect of particle size on bed-to-surface heat transfer [1,34,51,58-60]. Baskakov et al. [60] used two fluidized beds with diameters of 98 and 92 mm and two types of bed materials, which were corundum (mean diameter of 0.12, 0.32 and 0.5 mm) and slag beads (mean diameter of 0.65 mm). Three types of vertical heat transfer cylindrical tubes including rubber (15 and 30 mm in diameter) and stainless steel (30 mm in diameter) were used. Each of heat transfer probes was embedded with a 5 μm thick, $5\times10\ mm$ platinum strip. Carbon dioxide and helium at ambient temperature as well as air at temperatures ranging from 20 to 550 °C were used as fluidizing gas. They reported a non-monotonic trend for heat transfer coefficient as a function of particle size at ambient pressure and temperature (Figure 2-12) which was later also confirmed by Oka et al. [34] and Di Natale et al. [61]. It was observed that the heat transfer coefficient was initially increased with increasing particle size until a maxim value being reached. Then as particle size continued increasing, a decline in heat transfer coefficient occurred. In addition, the particle conduction heat transfer fell with the decline of overall convective heat transfer while the gas convection, both in emulsion and gas bubbles, started rising.

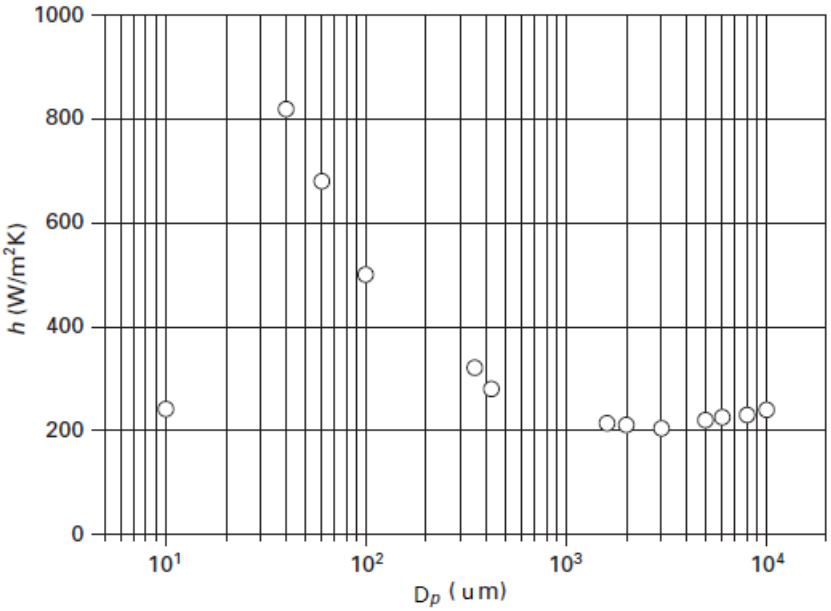

Figure 2-12: Effect of particle diameter on bed-to-surface heat transfer coefficient [61].

Baskakov et al. [60] also proposed a correlation for estimating contact thermal resistance R_k, as given in equation (2-5).

$$R_k = \frac{D_p}{2k_p} \tag{2-5}$$

where k_p is particle thermal conductivity.

According to Baskakov et al. [60], the contact thermal resistance almost reduced linearly with reduction of particle size (Figure 2-13).

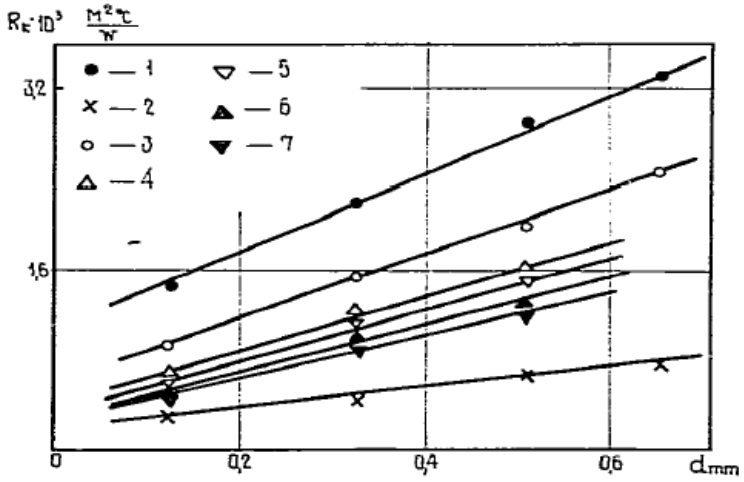

Figure 2-13: R_k vs particle diameter. 1-CO_2; 2-He at 20°C; 3, 4, 5, 6, 7-air at temperatures 20, 250, 350, 450, 550°C, respectively [60]

On the other hand, Decker et al. [65] reported that the thermal time constant τ, which was inversely proportional to the heat transfer rate between two contacting objects, was monotonically increased with particle size (Figure 2-14).

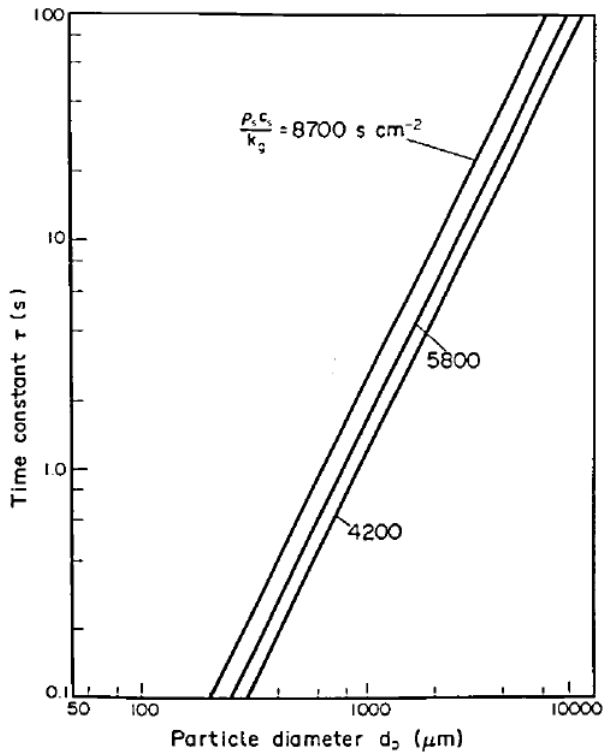

Figure 2-14: Variation of particle thermal time constant with particle diameter [65].

Baskakov et al. [60] suggested that the particle conductive component reduced with increasing particle size due to the rise of R_k and τ while the gas convection heat transfer was proportional to the power of 0.38 of particle diameter. Hence, as particle size increased the dominant heat transfer coefficient switched from particle conduction to gas convection. It was reported that for particle diameters greater than 500 μm the heat flow could hardly pass the first layer of particles [62]. Moreover, Grace [1] and Di Natale et al. [36] concluded that for large particles of which thermal time constant is larger than particle residence time, the heat transfer through gas surrounding the particle plays a fundamental role whereas for small particles of which thermal time constant is smaller than particle residence time, heat flow passed through several layers of particles resulting in a negligible thermal resistance of gas layers.

2.2.7 Correlations for Convective and Radiative Heat Transfer Estimation

Generally, models proposed for estimating the overall convective heat transfer coefficient could be categorized into 4 types of approaches [63]. The most common approach assumes that there is a gaseous boundary layer in-between the heat transfer surface and particles resulting in a thermal resistance. Particles scouring reduces the effective thickness of gaseous film and thus heat transfer enhances. The correlations derived from such approach follow a similar pattern which presents the heat transfer Nusselt number as a function of Prandtl number and a modified Reynolds number, with either particle diameter or tube diameter as characteristic length scale [65].

The second approach estimates gas convection and particle conduction heat transfer separately and combines them together as convective heat transfer.

The third approach is the packet theory which was firstly proposed by Mickley et al. [64]. It assumes that particle packet contacting the heat transfer surface for a period of time until being replaced by a fresh particle packets from a close infinite particle cluster [36]. The particle packets are assumed as a homogeneous emulsion phase with uniform bulk thermal properties obtained at minimum fluidization. For small particles, the packet theory accounts for the major portion of convective heat transfer, thus the overall convective heat transfer approximately equals to particle conductive heat transfer [63]. The last approach assumes an analogy between particle motion in fluidized bed and kinetic motion of gas molecules [63].

A summary of several models is presented in Table 2-1. Models considering radiative heat transfer coefficient in fluidized bed have been studied by many researchers [37,65,66] where two fundamental approaches have been developed. First approach estimates the radiant exchange between opaque gray bodies, referring to the heat transfer surface and bed particles, by using

Stefan-Boltzman equation. The second approach accounts for the radiant transfer process where particle layers [69] or particle packets [65] emitting, absorbing and scattering radiant photons while gas phase being transparent to thermal radiation. However, the second approach is somehow applicable when the radiative heat transfer is of significance.

Table 2-1. Summary of models on estimating overall convective and radiative bed-to-surface heat transfer coefficient.

No.	Author	Correlation	Conditions
Convective Heat Transfer			
1	Vreedenberg et al. [67]	$\frac{h_C D_T}{k_f} = 420\left(\frac{\rho_p}{\rho_f} Pr_f \frac{\mu_f^2}{g\rho_p^2 d_p^3}\right)^{0.3} Re_T^{0.3}$ $\frac{h_C D_T}{k_f} = 0.66 Pr_f^{0.3}\left(\frac{\rho_p(1-\varepsilon)}{\rho_f \varepsilon}\right)^{0.44} Re_T^{0.44}$	$\frac{\rho_p}{\rho_f} Re_p \geq 2550$ $\frac{\rho_p}{\rho_f} Re_p \leq 2050$
2	Mickley et al. [64]	$h_{pa} = 2\left[\frac{k_{pa}\rho_p c_{pp}(1-\varepsilon)_{pa}}{\pi\tau_{pa}}\right]^{1/2}$ $\tau_{pa} = \left[\frac{\sum\tau_i}{\sum(\tau_i)^{1/2}}\right]^2 \cong \frac{1-\delta_w}{f_b}$	
3	Borodulya et al. [68]	$\frac{h_C D_p}{k_f} = 0.85 Ar^{0.1}\left(\frac{\rho_p}{\rho_f}\right)^{0.14}\left(\frac{c_{pp}}{c_{pf}}\right)^{0.24}\varepsilon^{2/3} + 0.046 Re_p Pr_f\left(\frac{\varepsilon_p^{2/3}}{\varepsilon}\right)$ $+\frac{D_p}{\langle k_f\rangle}\frac{\sigma}{\frac{1}{E_W}+\frac{1}{E_b}-1}(T_b^2+T_W^2)(T_b+T_W)$	$0.1 < D_p < 6$ mm $293 \leq T_b, T_W \leq 1713$ K $0.1 < P < 10$ MPa $140 < Ar < 1.1 \times 10^7$

		$\langle k_f \rangle \; is \; k_f \; at \; T = \frac{T_W + T_b}{2}$	
4	Molerus et al. [50]	$\frac{h_C I}{k_f} = \frac{0.125\varepsilon_{p,mf}}{B_1\left[1 + B_2\left(\frac{k_g}{2c_{pp}\mu_f}\right)\right]} + 0.165 Pr_f^{1/3}\left(\frac{\rho_f}{\rho_p - \rho_f}\right)^{1/3}\left(\frac{1}{B_3}\right)$ $I = \left(\frac{\mu_f}{\rho_p - \rho_f}\right)^{2/3}\left(\frac{1}{g}\right)^{1/3}$ $B_1 = 1 + 33.3\left[\left(\frac{U_e \rho_p c_{pp}}{U_{mf} g k_f}\right)^{1/3} U_e\right]^{-1}$ $B_2 = 1 + 0.28\varepsilon_{p,mf}^2 U_e U_{mf}\left(\frac{\rho_f}{\rho_p - \rho_f}\right)^{1/2}\left(\frac{\rho_p c_{pp}}{g k_f}\right)^{2/3}$ $B_3 = 1 + 0.05\left(\frac{U_{mf}}{U_e}\right)$ $U_e = U - U_{mf}$	-

5	Chandran et al. [57]	$$h_{pa} = 2C\left[\frac{k_{pab}\rho_s c_{pp}(1-\varepsilon)_{pab}}{\pi\tau_{pa}}\right]^{1/2}$$ $$C = exp\left[\frac{-a_1}{Fo^{a_2+a_3 lnFo}}\right]$$ $$Fo = \frac{k_{pab}\tau_{pa}}{\rho_p c_{pp}(1-\varepsilon)_{pab}D_p^2}$$ $$a_1 = 0.213 + 0.117w + 0.041w^2$$ $$a_2 = 0.398 - 0.049w$$ $$a_3 = 0.022 - 0.003w$$ $$w = ln\left(\frac{k_{pab}}{k_g}\right)$$	
Radiative Heat transfer			

1	Molerus et al. [50]	$h_r = 4C_p\left(\frac{1}{\varepsilon_W}+\frac{1}{\varepsilon_b}-1\right)^{-1}\left[T_W+\frac{T_b-T_W}{2\left(1+k_g/2c_p\mu\right)}\right]^3\times\frac{1}{\left(1+k_g/2c_p\mu\right)}$	
2	Chen et al. [37]	$h_r=\frac{q_r}{T_b-T_W}=\frac{\sigma(T_b^4-T_W^4)}{(T_b-T_W)\left[\frac{1-E_b}{E_b}+1+\frac{1-E_W}{E_{\mathrm{W}}}\right]}$	

References

[1] J.R. Grace, Fluidized bed heat transfer, Handbook of Multiphase Flow, McGraw-Hill, Hemisphere, Washington, DC. 970 (1982).

[2] C.Y. Wen, Y.H. Yu, A generalized method for predicting the minimum fluidization velocity, AIChE J. (1966).

[3] J.F. Richardson, Incipient fluidization and particulate systems, Fluidization. 2 (1971).

[4] W. C. Yang, Handbook of fluidization and fluid-particle systems, CRC Press (2003).

[5] D. Geldart, Types of gas fluidization, Powder Technol. 7 (1973) 285–292.

[6] B. Bai, S. Gheorghiu, J.R. Van Ommen, J. Nijenhuis, M. O. Coppens, Characterization of the void size distribution in fluidized beds using statistics of pressure fluctuations, Powder Technol. 160 (2005) 81–92.

[7] L.R. Glicksman, W.K. Lord, M. Sakagami, Bubble properties in large-particle fluidized beds, Chem. Eng. Sci. 42 (1987) 479–491.

[8] H.T. Bi, A critical review of the complex pressure fluctuation phenomenon in gas-solids fluidized beds, Chem. Eng. Sci. 62 (2007) 3473–3493.

[9] M. Liu, Y. Zhang, H. Bi, J.R. Grace, Y. Zhu, Non-intrusive determination of bubble size in a gas-solid fluidized bed: An evaluation, Chem. Eng. Sci. 65 (2010) 3485–3493.

[10] J.F. Davidson, D. Harrison, R. Jackson, Fluidized particles, Cambridge University Press, (1964).

[11] T. Mckeen, T. Pugsley, Simulation and experimental validation of a freely bubbling bed of FCC catalyst, Powder Technol. 129 (2003) 139–152.

[12] B. Wu, G. Yu, C. Bellehumeur, A. Kantzas, Dynamic flow behavior measurements in gas–solid fluidized beds using different non-intrusive techniques and polyethylene powder, Flow Meas. Instrum. 18 (2007) 197–203.

[13] J. Van der Schaaf, J.R. Van Ommen, F. Takens, J.C. Schouten, C.M. Van den Bleek, Similarity between chaos analysis and frequency analysis of pressure fluctuations in fluidized beds, Chem. Eng. Sci. 59 (2004) 1829–1840.

[14] F.A. Zenz, N.A. Weil, A theoretical empirical approach to the mechanism of particle entrainment from fluidized beds, AIChE J. 4 (1958) 472–479.

[15] H. Do, J.R. Grace, R. Clift, Particle ejection and entrainment from fluidised beds, Powder Technol. 6 (1972) 195–200.

[16] A. Haider, O. Levenspiel, Drag coefficient and terminal velocity of spherical and nonspherical particles, Powder Technol. 58 (1989) 63–70.

[17] E. Hoekstra, S. Sookai, The effect of gas density on fluidized-bed entrainment, South African J. Chem. Eng. 19 (2014) 90–98.

[18] R. Clift, J.R. Grace, M.E. Weber, Particles, Acad. New York. (1978) 171–202.

[19] R. Turton, O. Levenspiel, A short note on the drag correlation for spheres, Powder Technol. 47 (1986) 83–86.

[20] T.P. Chen, S.C. Saxena, A theory of solids projection from a fluidized bed surface as a first step in the analysis of entrainment processes, Proc. Second Eng. Found. Conf. (1978) 151–156.

[21] S.E. George, Entrainment of particles from aggregative fluidized beds, AIChE Symp. Ser., (1978) 67–74.

[22] S.T. Pemberton, J.F. Davidson, Elutriation from fluidized beds—I. Particle ejection from the dense phase into the freeboard, Chem. Eng. Sci. 41 (1986) 243–251.

[23] M.H. Peters, L.-S. Fan, T.L. Sweeney, Study of particle ejections in the freeboard region of a fluidized bed with an image carrying probe, Chem. Eng. Sci. 38 (1983) 481–485.

[24] H. Hatano, M. Ishida, Study on the Entrainment of FCC Particles from a Fluidized Bed, Powder Technol. 35 (1983) 201–209.

[25] P.N. Rowe, D.J. Everett, Fluidized Bed Bubbles Viewed by X-Rays. Pt. 1. Experimental Details and The Interaction of Bubbles with Solid Surface, Trans Inst Chem Eng. 50 (1972) 42-48.

[26] W.R. Hager, W.J. Thomson, Bubble behavior around immersed tubes in a fluidized bed, AIChE Symp. Ser., (1973) 68.

[27] S. Fakhimi, D. Harrison, The voidage fraction near a horizontal tube immersed in a fluidized bed, Trans. Inst. Chem. Eng. 58 (1980) 125–131.

[28] N.M. Catipovic, Heat transfer to horizontal tubes in fluidized beds: experiment and theory, (1979).

[29] D.H. Glass, D. Harrison, Flow patterns near a solid obstacle in a fluidized bed, Chem. Eng. Sci. 19 (1964) 1001–1002.

[30] J. Wiman, A.-E. Almstedt, Hydrodynamics, erosion and heat transfer in a pressurized fluidized bed: influence of pressure, fluidization velocity, particle size and tube bank geometry, Chem. Eng. Sci. 52 (1997) 2677–2695.

[31] S.E. Olsson, J. Wiman, A.E. Almstedt, Hydrodynamics of a pressurized fluidized bed with

horizontal tubes: influence of pressure, fluidization velocity and tube-bank geometry, Chem. Eng. Sci. 50 (1995) 581–592.

[32] N. Muhlenov, B. Sazhin, V. Frolov, Calculation of Bubbling Fluidized Bed Apparatuses, Khimiya, Leningrad, (1986).

[33] A.P. Baskakov, Heat transfer in fluidized beds: Radiative heat transfer in fluidized beds, Fluidization, (1985) 465–472.

[34] Simeon N. Oka, Fluidized Bed Combustion, 1 (2004).

[35] C.Y. Wen, T.M. Chang, Particle to particle heat transfer in air fluidized beds, Proc. Int. Symp., (1967) 491.

[36] F. Di Natale, R. Nigro, Heat and mass transfer in fluidized bed combustion and gasification systems, Fluidized Bed Technologies for Near-Zero Emission Combustion and Gasification, (2013) 177-253.

[37] J.C. Chen, J.R. Grace, M.R. Golriz, Heat transfer in fluidized beds: Design methods, Powder Technol. (2005).

[38] O. Molerus, K.E. Wirth, Heat transfer in fluidized beds, Springer Science & Business Media, (2012).

[39] I. Sidorenko, M.J. Rhodes, Pressure Effects on Gas-Solid Fluidized Bed Behavior Pressure Effects on Gas-Solid Fluidized Bed Behavior, Int. J. Chem. Reactor Eng., 1.1 (2003).

[40] J.S.M. Botterill, M. Desai, Limiting factors in gas-fluidized bed heat transfer, Powder Technol. 6 (1972) 231–238.

[41] A.I.P. V.A. Borodulya, V.L. Ganzha, Heat transfer between fluidized bed of large particles

and horizontal tube bundles at high pressures, Int. J. Heat Mass Transf. 27 (1984) 1219–1225.

[42] N. Gelperin, V. Einshtein, Heat transfer in fluidized beds, Academic Press, (1971).

[43] A.O.O. Denloye, J.S.M. Botterill, Bed to surface heat transfer in a fluidized bed of large particles, Powder Technol. 19 (1978) 197–203.

[44] D.G. Traber, V.B. Sarkits, I.N. Mukhlenov, Heat-transfer for a suspended bed of catalyst to the heat-exchange surface, Zh. Prikl. Khim. 33 (1960) 2197–2205.

[45] L.B. Rabinovich, G.P. Sechenov, Characteristics of heat transfer from a surface to a fluidized bed under pressure, J. Eng. Phys. 22 (1972) 545–549.

[46] V.A. Borodulya, V.L. Ganzha, V.I. Kovenskii, Hydrodynamics and heat transfer in a fluidized bed under pressure, Minsk Sci. Technol. (1982).

[47] V.A. Borodulya, V.L. Ganzha, A.I. Podberezsky, Heat transfer berween fluidized bed of large particles and horizontal tube bundles at high pressures, Int. J. Heat Mass Transf. 27 (1984) 1219–1225.

[48] S.C. Saxena, V.L. Ganzha, Dependence of heat-transfer coefficient for immersed surfaces in a gas-fluidized bed on pressure, Powder Technol. 44 (1985) 115–124.

[49] S.C. Saxena, V.L. Ganzha, Heat transfer to immersed surfaces in gas-fluidized beds of large particles and powder characterization, Powder Technol. 39 (1984) 199–208.

[50] O. Molerus, W. Mattmann, Heat transfer in gas fluidized beds. Part 2: Dependence of heat transfer on gas velocity, Chem. Eng. Technol. 15 (1992) 240–244.

[51] F. Di Natale, A. Lancia, R. Nigro, A single particle model for surface-to-bed heat transfer in fluidized beds, Powder Technol. 187 (2008) 68–78.

[52] N.S. Grewal, S.C. Saxena, Maximum heat transfer coefficient between a horizontal tube and a gas-solid fluidized bed, Ind. Eng. Chem. Process Des. Dev. 20 (1981) 108–116.

[53] V.G. Einstein, N.I. Gelperin, Heat Transfer Between a Fluidized Bedand a Surface, Int. Chem. Eng. 6 (1966) 67–73.

[54] S.C. Saxena, N.S. Grewal, J.D. Gabor, S.S. Zabrodsky, D.M. Galershtein, Heat transfer between a gas fluidized bed and immersed tubes, Adv. Heat Transf. 14 (1979) 149–247.

[55] S.S. Zabrodsky, Y.G. Epanov, D.M. Galershtein, S.C. Saxena, A.K. Kolar, Heat transfer in a large-particle fluidized bed with immersed in-line and staggered bundles of horizontal smooth tubes, Int. J. Heat Mass Transf. 24 (1981) 571–579.

[56] J.A. Doherty, S.C. Saxena, Heat Transfer from Horizontal Tube Bundle in a Gas-Fluidized Bed, Proc. Eighth Int. Conf. Fluid. Combust, (1985) 1389–1398.

[57] R. Chandran, J.C. Chen, F.W. Staub, Local heat transfer coefficients around horizontal tubes in fluidized beds, J. Heat Transfer. 102 (1980) 152–157.

[58] D. Kunii, O. Levenspiel, A general equation for the heat-transfer coefficient at wall surfaces of gas/solid contactors, Ind. Eng. Chem. Res. 30 (1991) 136–141.

[59] N. Decker, L.R. Glicksman, Heat transfer in large particle fluidized beds, Int. J. Heat Mass Transf. 26 (1983) 1307–1320.

[60] A.P. Baskakov, B. V Berg, O.K. Vitt, N.F. Filippovsky, V.A. Kirakosyan, J.M. Goldobin, V.K. Maskaev, Heat transfer to objects immersed in fluidized beds, Powder Technol. 8 (1973) 273–282.

[61] F. Di Natale, A. Lancia, R. Nigro, Surface-to-bed heat transfer in fluidised beds of fine

particles, Powder Technol. 195 (2009) 135–142.

[62] J.S. BOTTERILL, Heat transfer to gas fluidized beds, Br. Chem. Eng. 11 (1966) 122.

[63] W.-C. Yang, M. Dekker, Handbook of fluidization and fluid-particle systems, CRC Press (2013).

[64] H.S. Mickley, D.F. Fairbanks, Mechanism of heat transfer to fluidized beds, AIChE J. 1 (1955) 374–384.

[65] J.C. CHEN, K.L. CHEN, Analysis of simultaneous radiative and conductive heat transfer in fluidized beds, Chem. Eng. Commun. 9 (1981) 255–271.

[66] O. Molerus, A. Burschka, S. Dietz, Particle migration at solid surfaces and heat transfer in bubbling fluidized beds-II. Prediction of heat transfer in bubbling fluidized beds, Chem. Eng. Sci. 50 (1995) 879–885.

[67] Vreedenberg, H. Heat transfer between a fluidized bed and a horizontal tube. Chemical Engineering Science , 9 (1958) 52-60.

[68] Borodulya, V., Teplitsky, Y., Sorokin, A., Markevich, I., Hassan, A., & Yeryomenko, T. Heat transfer between a surface and a fluidized bed: consideration of pressure and temperature effects. International Journal of Heat and Mass Transfer , 34 (1991) 47-53.

[69] Battacharya, Harrison D, Heat transfer in high temperature fluidized beds. Proc of Europ Conf Particle Tech, (1976).

[70] Kim, S.W., Ahn, J.Y., Kim, S.D., Lee, D.H., Heat transfer and bubble characteristics in a fluidized bed with immersed horizontal tube bundle." International Journal of Heat and Mass Transfer, 46.3 (2003) 399-409.

Chapter 3 Heat Transfer in a Pressurized Fluidized Bed with Continuous Addition of Fines

F. Li[a], E. Mielke[a], R.W. Hughes[b], M. Fitzsimmons[c], A. Macchi[a], P. Mehrani[a*]

[a] Department of Chemical and Biological Engineering, University of Ottawa, 161 Louis Pasteur Street, Ottawa, ON, Canada, K1N 6N5

[b] Natural Resources Canada, CanmetENERGY, 1 Haanel Drive, Ottawa, ON, Canada, K1A 1M1

[c] Gas Technology Institute-GTI, 5945 Canoga Avenue, Woodland Hills, CA, USA, 91367

[*]*Corresponding author email: poupak.mehrani@uottawa.ca; Tel: 1 (613) 562-5800 Ext. 6098; Fax: 1 (613) 562-5172*

3.1 Abstract

The goal of this work is to investigate the impact of pressure and presence of fine particles (i.e., a surrogate for pulverised fuel) on the overall surface-to-bed heat transfer coefficient in relation to an oxygen-fired pressurized fluidized bed combustor. Experiments were conducted in a pilot-scale fluidized bed with an inner diameter of 0.15 m under cold flow conditions. A tube bundle consisting of five horizontal staggered rows was completely submerged in the bed. One of the tubes was replaced by a heating cartridge housed in a hollowed copper rod. Five thermocouples distributed at 45º intervals along the copper rod circumference measured the surface temperature and ensured that local effects were included. The bed material was large glass beads of 1.0 mm in diameter while the fines were glass beads of 60 μm in diameter and thus susceptible to entrainment.

The fine particles were continuously fed to the fluidized bed and then captured downstream by a filter system. Fluidization was conducted at 101, 600 and 1200 kPa with excess gas velocities (U_g - U_{mf}) of 0.21, 0.29 and 0.51 m/s. Fine particle feed rates were 0, 9.5 and 14.4 kg/h. Two heating rod positions (2^{nd} row and 4^{th} row) were studies. Overall, the heat transfer coefficient approximately doubled when pressure was increased from 101 to 1200 kPa. At atmospheric conditions, where the slug flow regime occurred, the maximum heat transfer coefficient was at the bottom of the rod, while it moved to the side of the rod at high pressures where the bubbling regime occurred. As the heating rod moving from 2^{nd} row to the 4^{th} row, the averaged heat transfer coefficient increased by 18%, 9% and 6% at 101, 600 and 1200 kPa respectively. The addition of fine particles decreased the average heat transfer coefficient by 10 to 20 W/m^2 K where the averaged coefficients were approximately 220 and 450 W/m^{2}Kat 101 and 1200 kPa respectively, but there was no effect on the angular profile across the tube surface. The results showed that average heat transfer coefficients matched the correlation developed by Molerus et al. [29] within a 5% difference across all conditions when fines were not present.

Keywords: Heat transfer, Pressurized fluidized bed, Horizontal tube bundle

3.2 Introduction

Clean fossil fuel technologies that reach near zero CO_2 emissions are necessary to reduce the atmospheric CO_2 concentration and meet greenhouse gas reduction goals. Oxygen-fired pressurized fluidized bed combustion (Oxy-PFBC) with downstream CO_2 capture and storage is considered as a key approach to clean coal combustion. In such technology, the fluidized bed combustor operates at elevated pressures and houses an in-bed heat exchanger. To evaluate the performance of such technology, a 1 MW_{th} pilot plant was built and is currently under operation at NRCan CanmetENERGY in Ottawa, Ontario, Canada [1]. The Oxy-PFBC contains a bimodal particle mixture where large-sized bed material (e.g., dolomite or sand of ~ 1 mm in diameter) is used along with pulverized fuel particles (mean particle diameter of 70 to 100 μm). Pressurized operation as well as in-bed heat exchange are anticipated to result in greater heat transfer rates per unit surface area leading to reduced capital cost [2–4]. Hence, necessitating the need to accurately know the bed-to-surface heat transfer coefficient at these intensified operating conditions.

Bed-to-surface heat transfer (h_w) can be divided into three superimposed component/mechanisms: convective (h_{conv}), conductive (h_{cond}) and radiative (h_r) terms [5–7]. The conduction term refers to particle packets conducting heat while in contact with the surface, the convection term refers to heat transfer due to advection of gas in contact with the surface, and radiation is from radiant heat transfer. Moreover, the convective and the conductive components are often grouped together as an overall convective term, h_C [8–10]. Alternatively, in a bubbling fluidized bed, overall convective heat transfer (h_C) can be represented as gaseous convection (h_l) during bubble contact (lean phase), and conduction/convection (h_d) during particle contact (dense phase) resulting in the nomenclature shown in Equation (1).

$$h_W = h_{conv} + h_{cond} + h_r = h_C + h_r = f_l h_l + (1 - f_l) h_d + h_r \quad (3\text{-}1)$$

There have been several tube-to-bed heat transfer studies covering a large range of fluidization conditions including temperature, pressure, gas and bed material physical properties, tube and tube bank geometries, and gas superficial velocity [11–15]. Efforts have been made in correlating pressure and bed-to-surface heat transfer, with h_C generally increasing with a rise in pressure for particles larger than 0.6 mm [14,16–19]. From the particle classification of Saxena and Ganzha [20], they suggests that heat transfer by particle conduction dominates for particles in group I ($3.55 < Ar < 21700$) and IIA ($21700 < Ar < 130000$) where a rise in pressure increases the gas thermal conductivity as well as produces smaller bubbles and thus greater particle frequency renewal at the surface, which leads to a minor increase in conductive heat transfer (h_{cond}). For particles in groups IIB ($1.3\times10^5 < Ar < 1.6\times10^6$) and III ($Ar > 1.6\times10^6$), the effect of pressure on h_C is due to the dominant contribution of gas convection (h_{conv}) which increases with greater gas density. It is also reported that an increase in superficial gas velocity results in a rise in heat transfer rate until a maximum value is reached, followed by a decline with further increase in velocity [17,19–21]. At the incipient fluidization point, there is a large increase of heat transfer due to particle mixing. A continued rise in gas velocity further increases the particle renewal frequency at the surface and the gas convection, but decreases the particle concentration due to the bed expansion. This leads to an optimum heat transfer value for a given gas-solid fluidization system. Moreover, an increase in heat transfer coefficient was reported as the heating source location was varied within a tube bundle from a bottom row to an inner row [19].

All aforementioned studies used bed material having a relatively narrow or single mode size distribution. The aim of this work was thus to extend the above literature knowledge base by measuring and modeling the combined convective and conductive tube-to-bed heat transfer

coefficient for both bimodal and single mode size distribution under cold-flow operating conditions similar to those of an Oxy-PFBC. Local instantaneous and time-averaged heat transfer data for a tube within a tube bank is reported as a function of operating pressure, superficial gas velocity and fines feed rate.

3.3 Experimental Apparatus and Procedure

The cold-flow fluidized bed (Figure 3-1) was a 3 m tall stainless-steel column with an inner diameter of 0.15 m. The distributor plate consisted of two perforated stainless steel plates with a 45 μm mesh in between. The top plate had 61 holes of 6 mm in diameter whereas the bottom plate had 61 holes of 4 mm in diameter. The fluidized bed was operated up to a pressure of 1200 kPa using building air and/or compressed air cylinders and a centrifugal compressor for the gas to be recirculated in a closed loop. The gas flow at the exit of the compressor was sent to a plate heat exchanger, which used chilled water as the thermal medium, in order to maintain the gas temperature constant at the entrance of the column. The gas flowrate was monitored using an orifice place meter for atmospheric operation and a vortex meter for pressurized operation. The operating pressure was measured by a gauge pressure transducer and the pressure drop across the fluidized bed was measured by a differential pressure transducer.

For the commercial Oxy-PFBC, a potential bed material is either dolomite or sand with an average diameter of 1 mm and a density ranging 2500-3000 kg/m^3 and a potential pulverized fuel is coal with a particle mean diameter ranging 0.07-0.1 mm and a density of 1500 kg/m^3. The cold-flow experimental bed material and fines were selected to be glass beads of 2500 kg/m^3 in density and 1 mm (Geldart group D) and 60 μm in average diameter, respectively. As shown in Table 3-1, the experimental operating conditions as well as the bed material properties for the cold-flow tests were chosen to simulate the Oxy-PFBC at high pressures and temperatures according to the scale

up principles mentioned by Glicksman et al. [22, 23] while relaxing geometric similitude relative to column cross-sectional shape (rectangular vs circular). Table 3-2 shows that the fine particles were chosen to achieve similar estimated terminal velocities [24,25] to the pulverized fuel.

Table 3-1. Bed material properties in the Oxy-PFBC and cold-flow experimental unit. Air properties were estimated at 23°C for 101 and 1200 kPa for the cold flow operation, whereas at commercial conditions the gaseous mixture was composed of 1/3 vol. H_2O and 2/3 vol. CO_2 at 1200 kPa and 850°C .

		Ar	Mean D_p	$\frac{U}{U_{mf}}$	$\frac{H}{D_C}$	$\frac{\rho_p}{\rho_f}$	$\frac{U^2}{g^2}$	Particle Sphericity
		(-)	(mm)	(-)	(-)	(-)	(-)	(-)
Bed material	Oxy-PFBC	$1.7\times10^5 - 2.2\times10^5$	1	2.0-3.5	3	551-705	0.0023 - 0.0063	0.85
	Cold-flow experimental unit	$8.5\times10^4 - 1\times10^6$	1	1.35 - 3.2		2123-177		1

Table 3-2. Fine particle properties in the Oxy-PFBC and cold-flow experimental unit. Air properties were estimated at 23°C for 101 and 1200 kPa for cold flow operation, whereas at commercial conditions the gaseous mixture was composed of 1/3 vol. H_2O and 2/3 vol. CO_2 at 1200 kPa and 850°C

		P	T	Mean D_p	ρ_p	Ar	U_t
		kPa	K	(mm)	(kg/m^3)	(-)	(m/s)
Fines	Oxy-PFBC	1200	1123.15	0.07-0.1	1500	0 – 100	0.13-0.22
	Cold-flow experimental unit	101 - 1200	296.15	0.06	2500	10 - 200	0.16 – 0.23

A screw auger was placed inside a pressure vessel and used for the continuous feeding of fines. The feeder discharge was connected to the fluidization column by a 6.35 mm diameter stainless steel pneumatic conveying line using air from a cylinder. At the column outlet, a bag filter system consisting of two parallel filters captured the entrained fines. Filters had 95% capture efficiency for 10 μm in diameter particles as per manufacturer design specification. A three-way valve was used to switch gas flow from one filter to another so that continuous operation was achieved.

A horizontal tube bundle, geometrically similar to that of the pilot scale Oxy-PFBC, was lowered into the fluidized bed. The tube bundle consisted of five rows of staggered horizontal aluminum tubes housed in a stainless steel cylindrical sleeve with a total height of 0.50 m and an inner diameter slightly smaller than that of the column (Figure 3-2). The first row of tubes started 0.22 m above the distributor plate and all tubes were arranged such that the relative horizontal and vertical pitches (S_H/D_t and S_V/D_t) were above 2 and 1.5, respectively. No further geometrical detail can be given due to the proprietary design. An opening on the side of the sleeve allowed for the pneumatic line to access the column so that the fines are injected at the column center. For heat transfer measurements, the heating rod was positioned along the central vertical axis, replacing an aluminum tube in the bottom-row (the 2nd row) or the one in the inner-row (the 4th row) as shown in Figure 3-2. The heating rod was a 101.6 mm long copper rod with 19 mm of PTFE insulation on each end in order to limit longitudinal heat transfer. The rod was milled out and a 900 W (60 V) cartridge heater was installed inside (Figure 3-3a). K-type thermocouples, measuring the temperature at a frequency of 90 Hz, were installed at five different locations along the circumference, 45º apart (Figure 3-3b). The thermocouple response time constant was estimated at 0.3 s. Power was supplied to the cartridge heater by a switching DC power supply. The power

setting resulted in a surface temperature (T_t) of ~323.15 K (or a $\Delta T = T_t - T_b \approx 25$ K), which allows an acceptable experimental accuracy on the calculation of h_C.

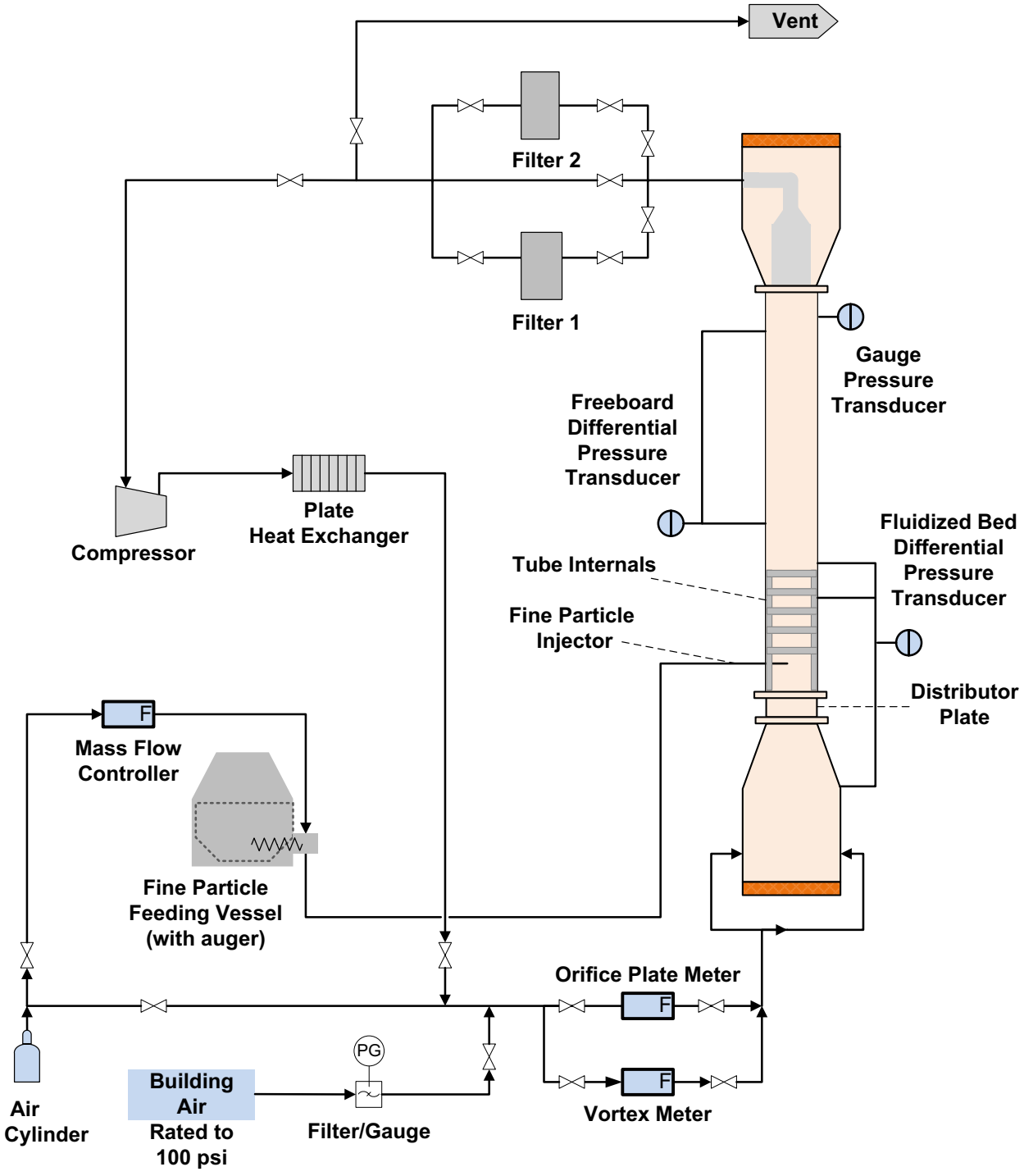

Figure 3-1: Schematic of the fluidization system.

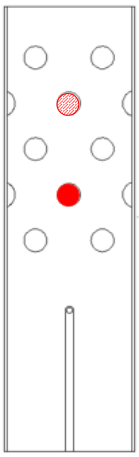

Figure 3-2: Schematic of the tube bank and the sleeve housing the heating rod at 2nd row (solid circle) and 4th row (shaded circle)

a)

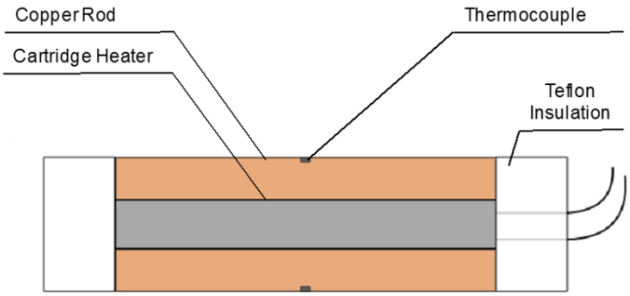

b)

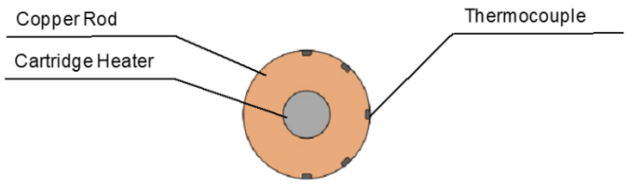

Figure 3-3: heating rod **(a)** side view, and **(b)** cross view showing thermocouple locations

3.4 Measurement method

Through supplying the copper rod with a constant power (*IV*) and monitoring bed and rod surface temperature (T_b & T_t), the local time-averaged convective heat transfer coefficient at a given thermocouple, *i* ($h_{C,i}$) was determined by Equation (3-2).

$$h_{C,i} = \frac{IV}{A\left(T_{t,i} - T_b\right)} \tag{3-2}$$

In order to obtain the average value of h_C across the entire tube surface, symmetry of the tube was assumed by numerically repeating the values for thermocouples 2 to 4. For this reason, h_C was calculated as in Equation (3-3).

$$h_C = \frac{\sum_1^5 h_{C,i} + \sum_2^4 h_{C,i}}{5 + 3} \tag{3-3}$$

The time-series analysis of the local surface temperature signal was performed for a duration of 8 seconds at steady-state. For comparison convenience, the instantaneous local tube temperature $T^*_{t,i}$ was normalized by its time-averaged value as in Equation (3-4).

$$T^*_{rel,i} = \frac{\left(T^*_{t,i} - T_{t,i}\right)}{T_{t,i}} \tag{3-4}$$

The heat transfer coefficient was measured under a variety of operating pressures, gas velocities, and fines feed rates.

Table 3-3 summarizes the conditions tested and also shows the value of U/U_{mf} at various pressures for equivalent excess gas velocity, U_e. Each operating condition was attempted two to five times to estimate the precision of the data and the resulting maximum value of the coefficient of variation (standard deviation divided by the average) for any given operating condition was 0.011. The differential pressure measurement across the whole bed along with Equation (3-5) were used to

estimate the average bubble size, which permitted to qualitatively compare bubble dynamics for the different operating conditions. Here, the proportionality constant is 1 as suggested by Liu et al. [26].

$$d_{B,\Delta P} \propto \frac{\sigma_{\Delta P}}{\rho_p g(1-\varepsilon_{mf})} \tag{3-5}$$

For the experiments without fines, the bed and local surface temperatures were collected for 2 minutes once the system reached steady-state. For experiments with fines fed, a three-stage procedure was followed. At first, the fines were collected in the first filter bag for 8 minutes to allow the system to reach steady state. Then the solid-gas flow was switched to the second filter bag at which point the bed and local surface temperatures were collected for 10 minutes. Finally, the injection of fines stopped, and the flow was switched to a third filter bag that collected for at least 20 minutes the fines that remained within the bed.

Table 3-3. Operating conditions tested in this work.

Pressure (kPa)	U/U_{mf}	U_e **(m/s)**	**Fines Feed Rate (kg/h)**	**Heating Rod Location (-)**
101	1.35	0.21	0	2nd row
101	1.5	0.29	0	2nd row
101	1.9	0.51	0	2nd row
600	1.9	0.29	0	2nd row
1200	1.9	0.21	0	2nd row
1200	2.2	0.29	0	2nd row
1200	3.2	0.51	0	2nd row
101	1.35	0.21	9.5	2nd row

101	1.5	0.29	9.5	2nd row
101	1.9	0.51	9.5	2nd row
600	1.9	0.29	9.5	2nd row
1200	1.9	0.21	9.5	2nd row
1200	2.2	0.29	9.5	2nd row
1200	3.2	0.51	9.5	2nd row
1200	2.2	0.29	14.4	2nd row
101	1.5	0.29	0	4th row
101	1.5	0.29	9.5	4th row
1200	2.2	0.29	0	4th row
1200	2.2	0.29	9.5	4th row

3.5 Results and Discussion

3.5.1 Effect of Gas Velocity at Various Pressures

The average convective heat transfer coefficient was compared at various excess gas velocities (0.21 to 0.51 m/s) and pressures (101, 600 kPa and 1200 kPa) for the lower heater tube location. Results in Figure 3-4 show that pressure had a positive impact on the heat transfer coefficient. An increase in pressure from atmospheric to 600 kPa nearly doubled the heat transfer coefficient and increasing the pressure from 600 to 1200 kPa further raised it by roughly 30%. Figure 3-4 also shows that increasing the gas velocity reduced the heat transfer coefficient, for the range of gas velocity examined here, which is expected for Geldart group D particles that attain their maximum heat transfer coefficient relatively shortly after U_{mf} [7,27,28]. While an increase in gas velocity

positively impacts heat transfer via gas convection, the reduction in heat transfer via particle conduction due to the bed expansion has a greater effect on the overall h_C.

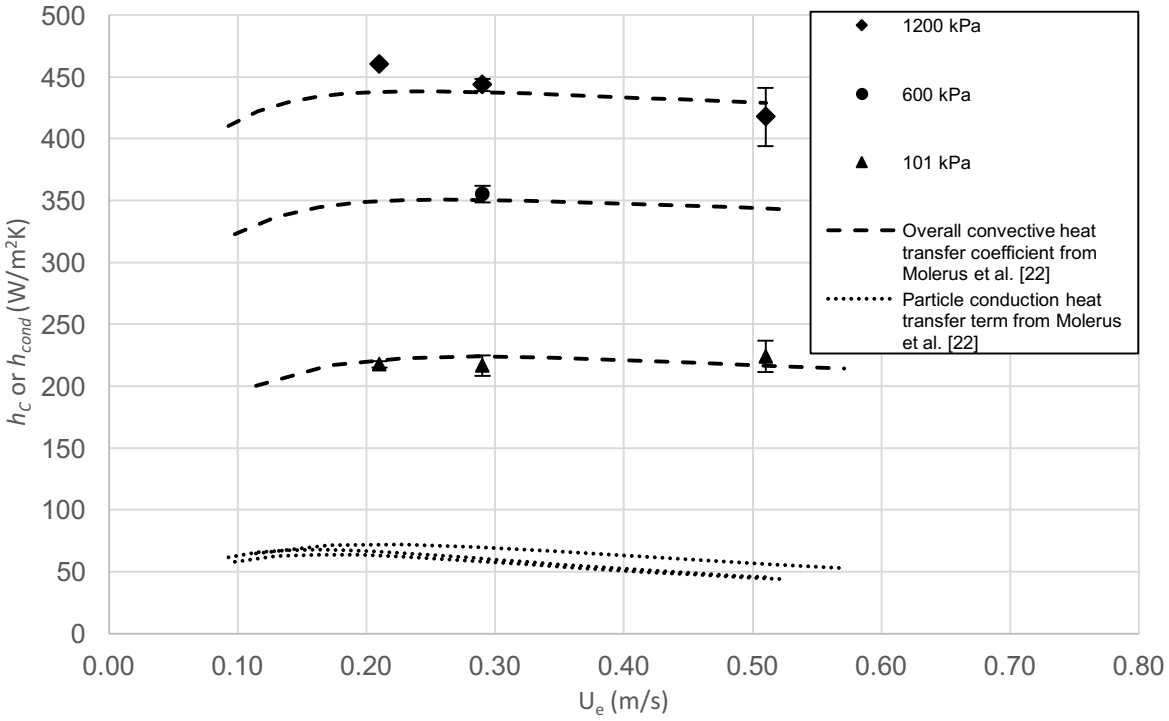

Figure 3-4: Experimental h_C for various U_e and pressures. Lines are the estimates of h_C and h_{cond} from the correlation of Molerus et al. [29]

Interestingly, the measured average heat transfer coefficients matched the comprehensive single tube model developed by Molerus et al. [29] within a 5% difference for all conditions. Borodulya et al. [30] and Doherty and Saxena [31] found that h_C is insensitive to horizontal and vertical tube pitches in a staggered horizontal tube bundle for $S_H \geq 2\ D_t$ and $S_V \geq 1.5\ D_t$ when fluidizing large particles. Zabrodsky et al [14] also compared heat transfer between a single tube and a horizontal in-lined tube bundle for large particles and concluded that h_C for a single tube coincides with that of the bundle as long as the horizontal and vertical pitches between the tubes were larger than $3.3\ D_t$. Therefore, the Molerus et al. [29] correlation is applicable here since in this work the tube bundle horizontal and vertical pitches were greater than $2D_t$ and $1.5D_t$, respectively to allow

free movement of the solids as well as the heating rod being located in the 2nd row where there was no other tube located directly beneath. In addition, the Molerus et al. [29] model suggests that heat transfer via particle conduction is not a strong function of pressure and hence the rise in h_C is primarily due to increased heat transfer via gas convection resulting from the greater gas density at higher pressure. Moreover, according to this model, particle conduction accounts for no more than 40% of the heat transferred. As such, the primary mechanism of heat transfer is via gas convection for the selected operating conditions, which is expected for bed material with an Ar number above 8×10^4.

It is important to note that the cold flow tests performed in this work do not allow the study of radiative heat transfer. However, Flamant et al [32] concluded that radiative heat transfer is likely significant at temperatures greater than 800 K for Geldart Group D particles. Hence, the estimation of the radiative term is important in relation to the Oxy-PFBC operated at 1123 K. Correlations proposed by Molerus et al [29] and Chen et al.[8] were used to estimate the radiative heat transfer coefficient. Chen et al. [8] considered radiation transport as an exchange between opaque gray bodies separated by an inert medium. The emissivity of dolomite and the aluminum tube surface are estimated as 0.958 [33] and 0.7 [8], respectively. The temperature of tube wall with water as cooling fluid ranges from 373.15 to 423.15 K as reported by Oka [34]. For all fluidization conditions, the resulting radiative contribution to the overall heat transfer coefficient is estimated to be less than 3 and 12% based on the Molerus et al. [29] and Chen et al. [8] models, respectively. Molerus et al. [29] assumed that only the first layer of particles near the surface played a significant role in radiation transfer, leading to a different estimate than that obtained by Chen et al. [8] model. Ultitmately, both Chen et al. [8] and Molerus et al [29] approaches suggest that radiative contribution to the overall heat transfer coefficient is minor at the selected Oxy-PFBC conditions.

Figure 3-5 presents the local heat transfer coefficient across the angular profile of the heated tube surface located in the 2nd row. In order to compare all results on the same basis, the local values were normalized to the spatially averaged heat transfer coefficient, as shown in Equation (3-6).

$$h_{rel,i} = \frac{(h_{C,i} - h_C)}{h_C} \times 100\% \quad (3\text{-}6)$$

Although there is an angular variation in the heat transfer coefficient from thermocouple 1 to 5, it is minor being always within 3% of the mean. However, operating pressure seems to play a significant role on the location of the maximum heat transfer coefficient as it is shifted from thermocouple 1 (the bottom of the heating rod) to 3 (the side of the heating rod) when pressure is increased. This is likely due to the resulting fluidization flow regime change for these operating conditions. At atmospheric pressure, the average gas bubble size was estimated to be 0.11 m, thus indicating a slug flow regime. Large slug-shape bubbles rise and push clusters of particles into the bottom of the tube thereby increasing the heat transfer rate at thermocouple position 1 relative to the rest of the rod. In contrast, the average bubble size at 1200 kPa was estimated to be 0.03 m and thus bubbly flow occurred. These smaller bubbles are more likely to pass in between the tubes without direct contact or breakup, increasing heat transfer via particle conduction at the side of the tube (i.e., at thermocouple 3). Thermocouple 4 registered the lowest heat transfer coefficient at each operating pressure. This is likely due to the particles hitting the bottom of the tube and bouncing away from the 4th thermocouple position, which then locally reduces the particle turnover and particle concentration. Results in Figure 3-5 also indicate that the range of excess gas velocity does not significantly affect the angular trend in local heat transfer coefficients since, for a given pressure, the flow regime did not change.

The angular position of the local minimum heat transfer coefficient in this work is consistently at thermocouple 4. This slightly differs from the very top position (i.e., thermocouple position 5) generally reported by various authors [19,35] who observed that there is a region above the tube where particles move slowly or not at all resulting in low surface renewal frequency and heat transfer coefficients. Although, the angular heat transfer was still fairly uniform in this work, these specific results will be used to better anticipate the location of greater tube erosion in the Oxy-PFBC as it too is a function of the local particle surface renewal frequency and concentration.

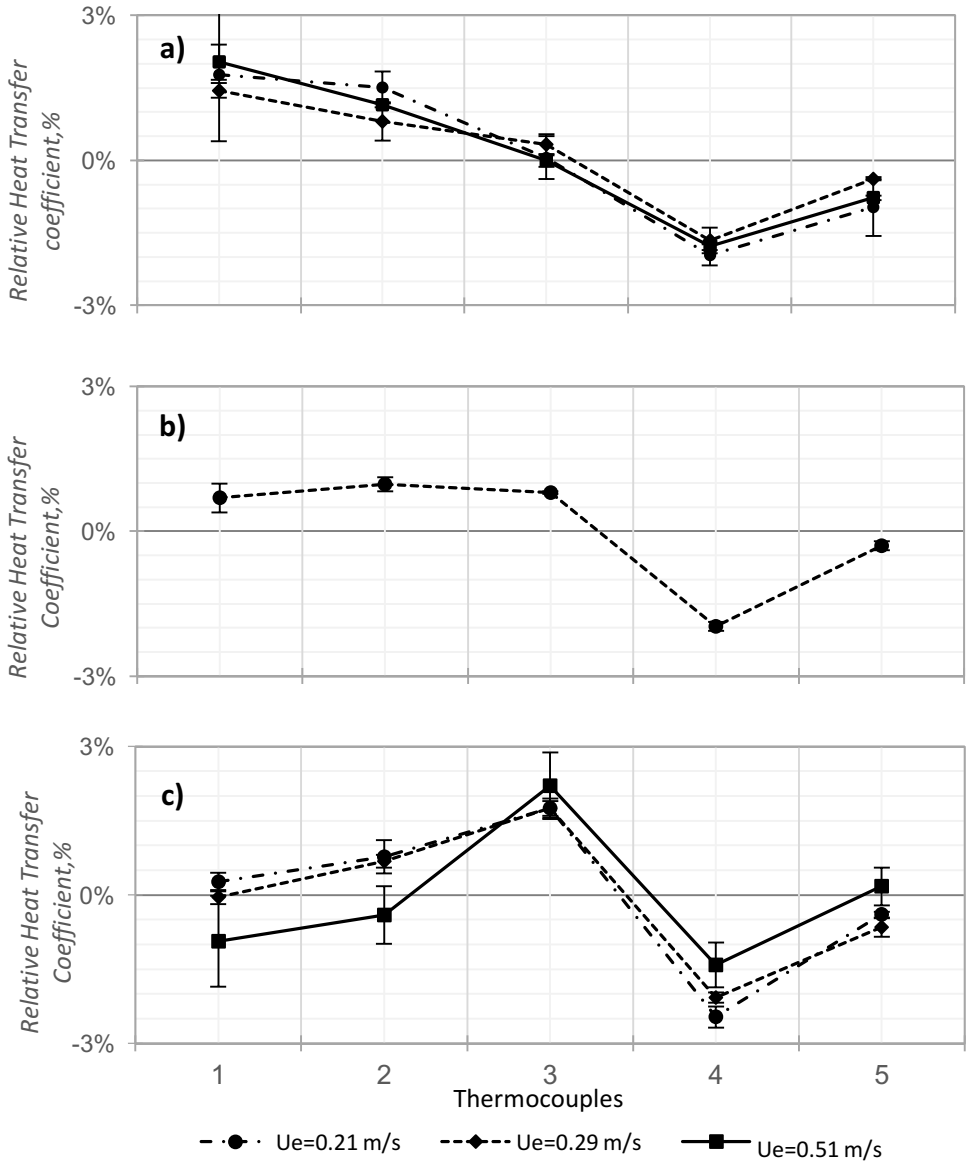

Figure 3-5: Relative heat transfer coefficient across the heating rod surface at a) 101 kPa, b) 600 kPa, and c) 1200 kPaat various U_e without fines.

Figure 3-6 and Figure 3-7 present a portion of the time series from the bed pressure drop and local surface temperature at an excess gas velocity of 0.29 m/s and at 101 and 1200 kPa in pressure, respectively for the lower heating rod location. Visual observation of the differential pressure signals between the two operating conditions suggest different bubble dynamics, with a greater frequency and lower amplitude signal at elevated pressure representing smaller bubbles. Although variations in the local time-averaged normalized relative temperatures are less than 1% for all

thermocouple positions at both operating conditions, visual observations indicate that the signal is more periodic at atmospheric than elevated pressure, especially for thermocouple positions 3 to 5. Corroborating with the pressure drop signal, the large slugs formed at atmospheric pressure likely rise and hit the heating cartridge periodically while the smaller bubbles at a pressure of 1200 kPa contact the heating surface more frequently and in an aperiodic manner. Olsson and Almstedt [36] compared capacitance probe with heat flux sensor signals, and the lean and dense phase presented similar relative trends in both signals. They also observed that an elevated pressure lead to more rapid fluctuations between the lean and dense phase contributions to the signals than at atmospheric pressure. Furthermore, the signals from the top of the tube show a less marked distinction between lean and dense phases than the signals from the bottom of the tube.

The power spectrums of the time series for all local relative surface temperatures at 101 kPa and 1200 kPa are respectively shown in Figure 3-8 and Figure 3-9 for the lower heating rod location. At atmospheric pressure, the power spectrums show distinguishable peak frequencies at around 1 to 1.2Hz as well as at 0.1 to 0.25Hz, although the latter frequency becomes less prominent as thermocouple position goes from 1 to 5. The power spectrums at elevated pressure shows a broader frequency distribution, which suggests the presence of a wider bubble size distribution.

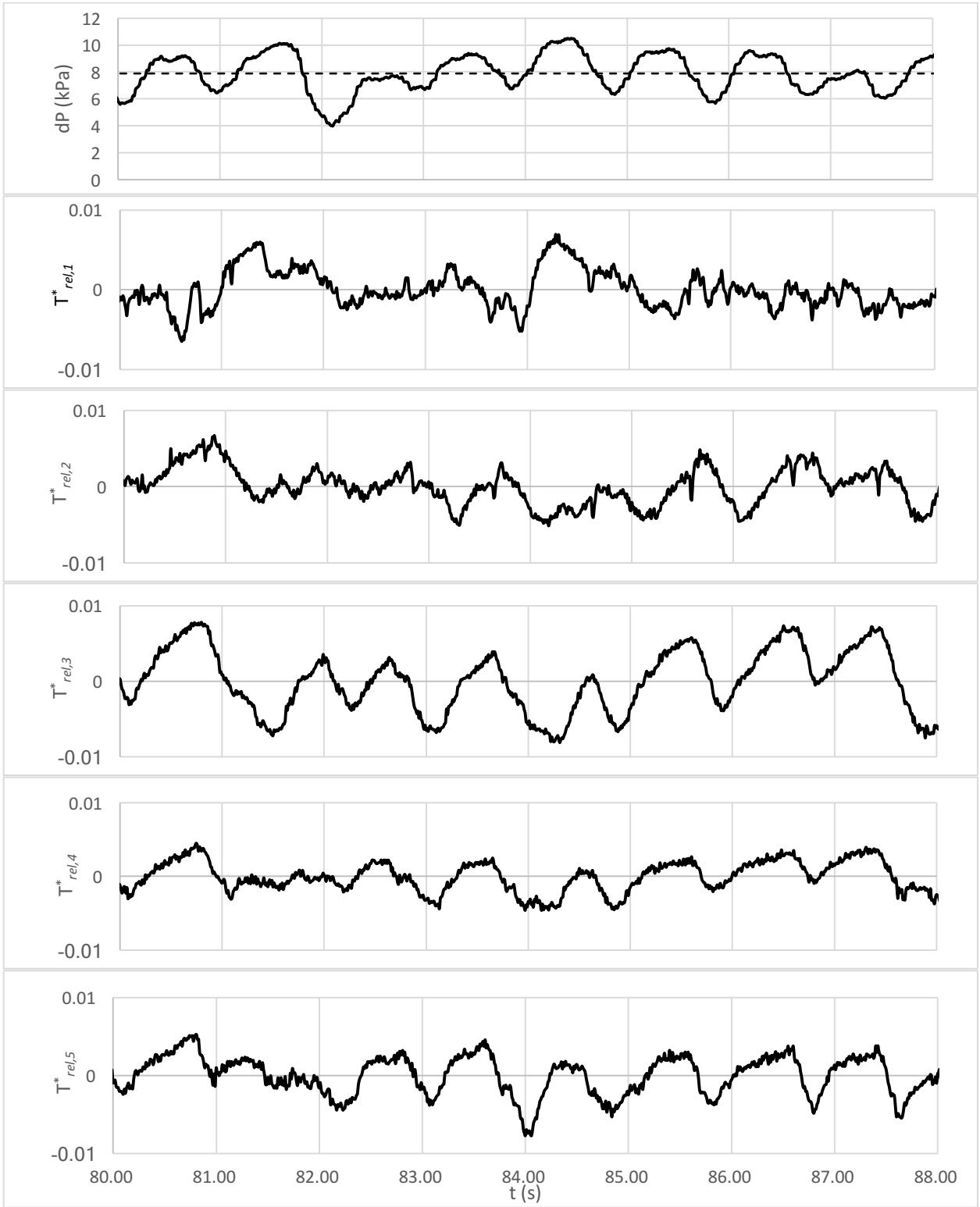

Figure 3-6: Local Temperature Relative Error and differential pressure time – series signal at U_e = 0.29 m/s without fine particle injection at 101 kPa condition.

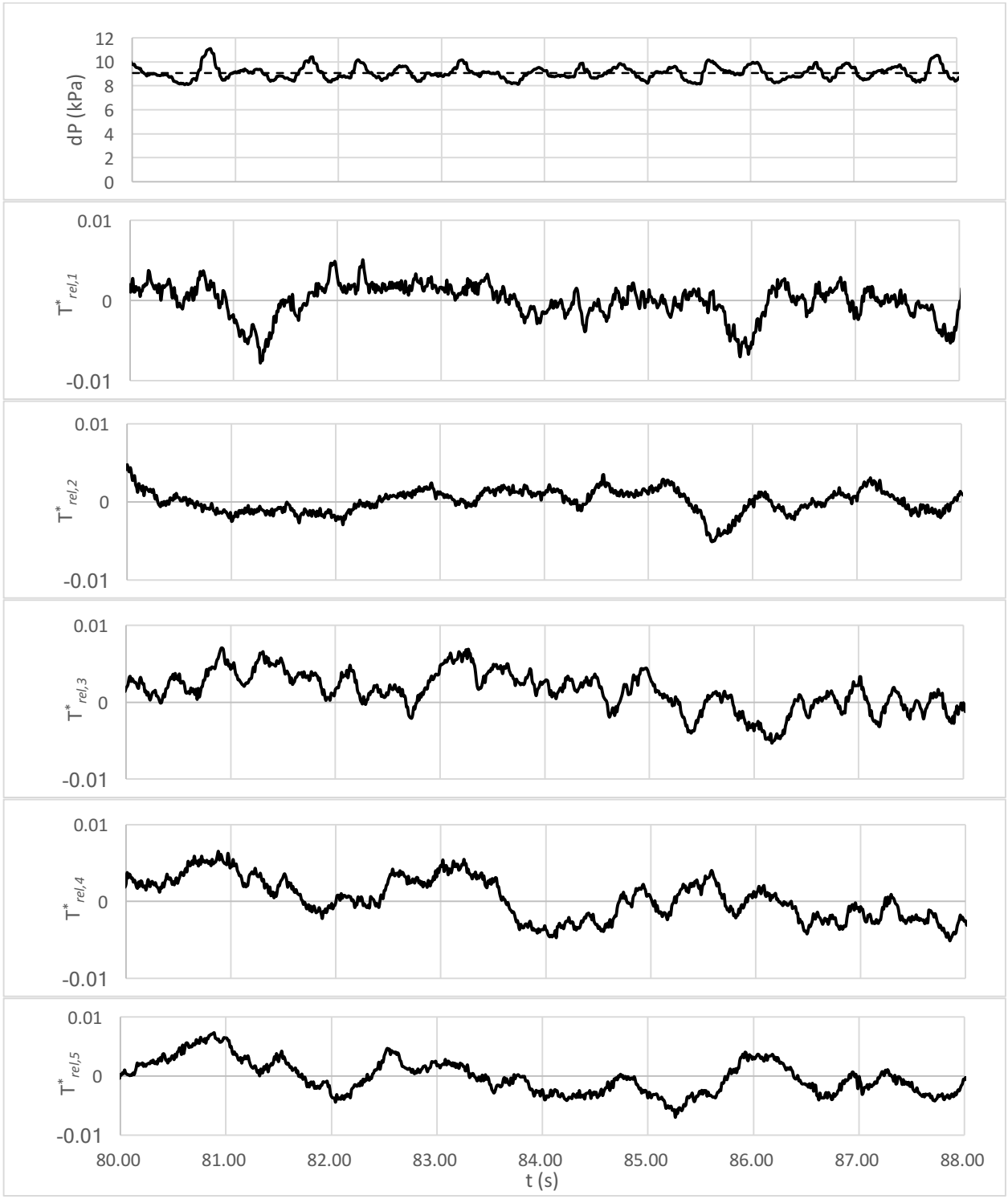

Figure 3-7: Local Temperature Relative Error and differential pressure time series signal at U_e = 0.29 m/s without fine particle injection at 1200 kPa condition.

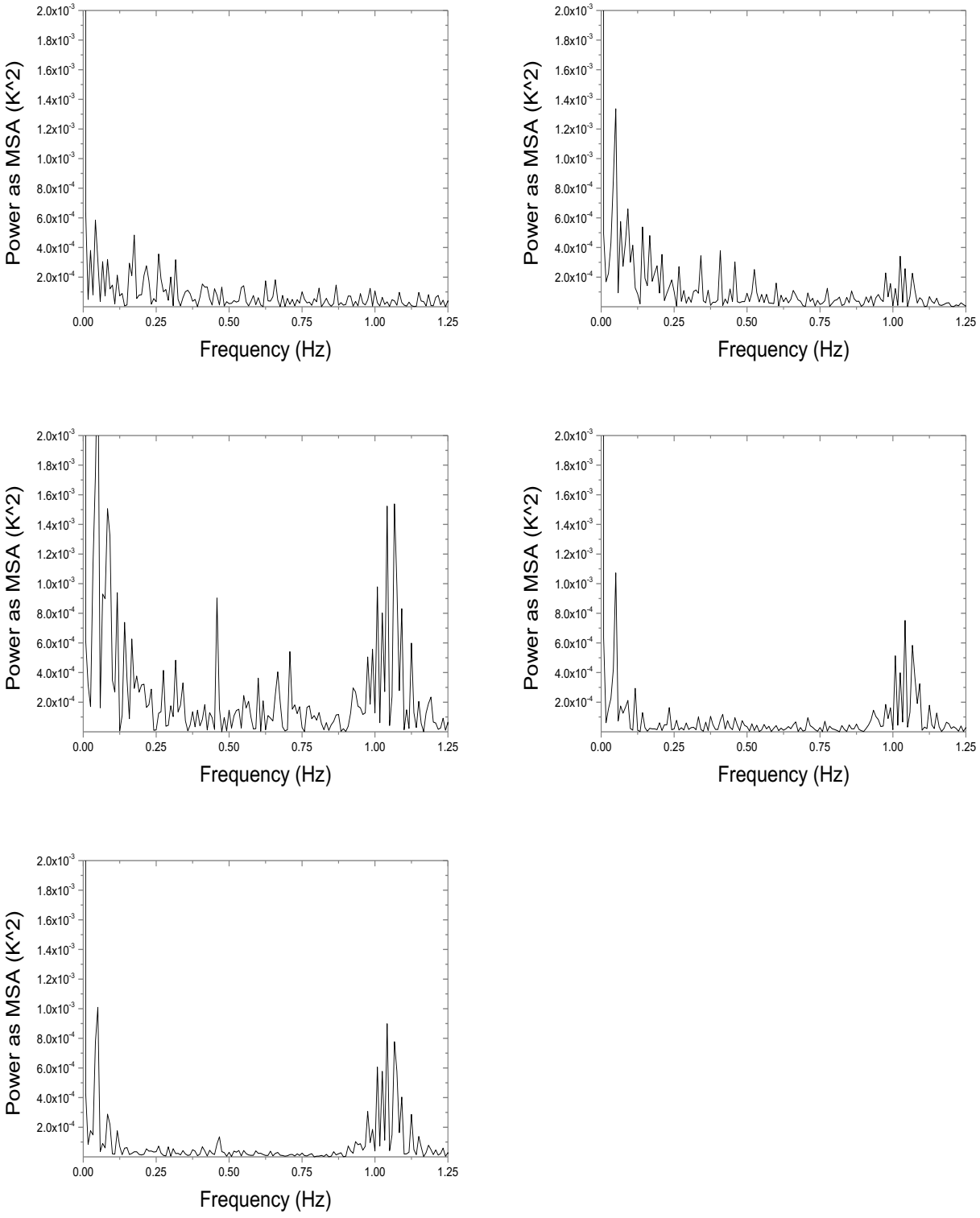

Figure 3-8: Power Spectrum of local temperature signal from 1st thermocouple to 5th thermocouple at U_e = 0.29 m/s without fine particle injection at 101 kPa.

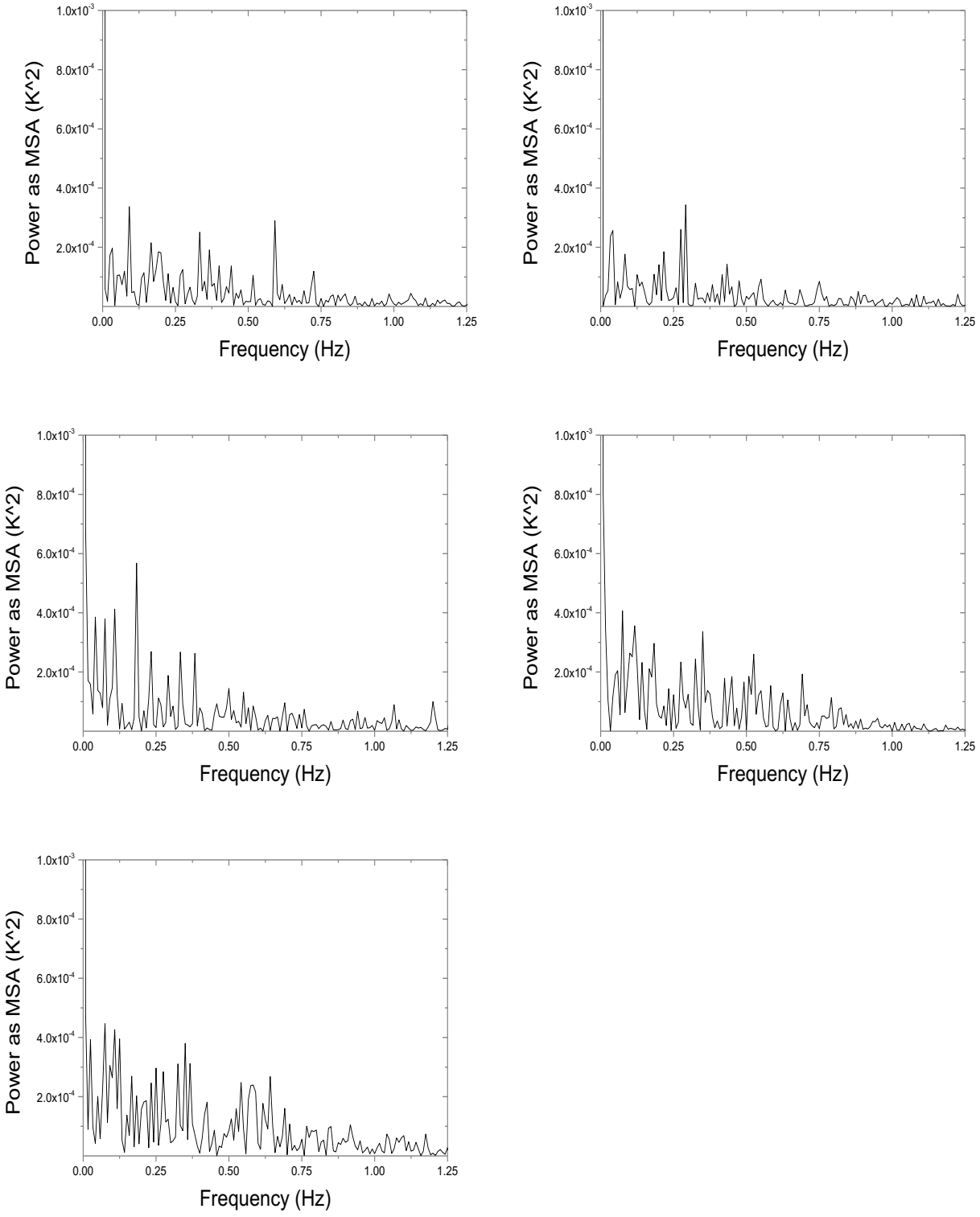

Figure 3-9: Power Spectrum of local temperature signal from 1st thermocouple to 5th thermocouple at U_e = 0.29m/s without fine particle injection at 1200 kPa.

3.5.2 Effect of Addition of Fines

Fine particles were continuously injected into the fluidized bed below the tube bundle at a rate of 9.5 and 14.5 kg/h in order to test the impact of a bimodal particle size distribution on the tube-to-bed heat transfer coefficient, as would be the case with the Oxy-PFBC. For the various operating conditions tested, the resulting fines mass fraction in the fluidized bed was between 0.5 to 5% based on the mass collected in the final filter once the fines feed was stopped. Moreover, based on the mass of fines collected in the final filter and the established steady-state fines mass flow rate, the resulting fines mean residence times in the fluidized bed was estimated to be between 25 and 250 seconds across all conditions. Figure 3-10 shows that the fines did not impact the local trends in angular heat transfer coefficients along the rod circumference. Whereas, in Figure 3-11, the fines decreased h_C by around $10 \sim 20$ W/m^2 K across all operation conditions. The power spectrum of the local temperature times series with fine particles present (Figure 3-12) is similar to fines-free experiments (Figure 3-8), which suggests that bubbles dynamics and two-phase heterogeneous morphology remain relatively constant. As such, Vreman [37] reported that the addition of fines can decrease the gas-phase turbulence for particle-laden flow, which would result in lowering the heat transfer coefficient when the mechanism of heat transfer is primarily via gas convection such as here. However, as the fines concentration increases, benefits to heat transfer via particle conduction should eventually lead to an increase in the overall convective heat transfer coefficient.

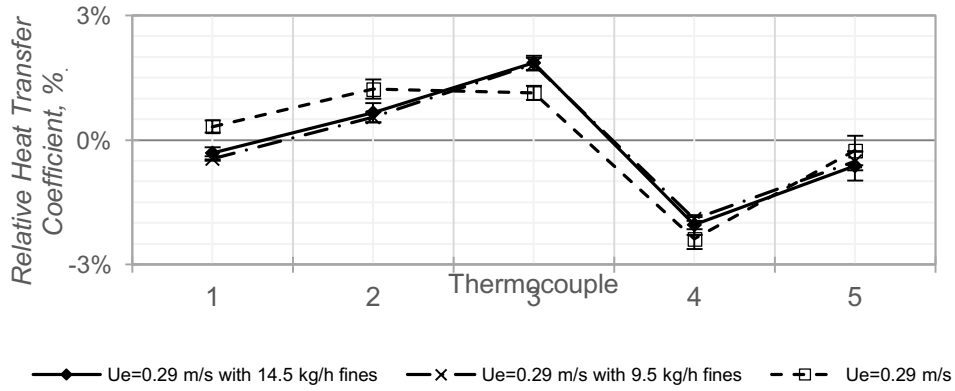

Figure 3-10: Relative heat transfer coefficient across the rod surface at 1200 kPa at U_e= 0.29m/s with 9.5 kg/h fines, 14.4 kg/h fines and without fines

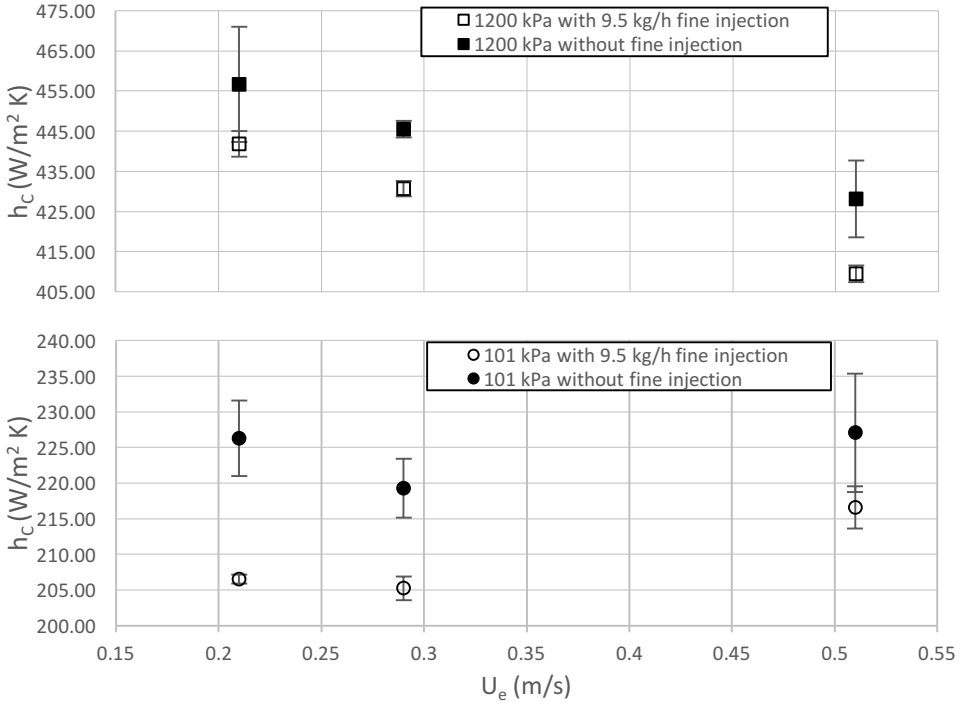

Figure 3-11: Effect of fine additions in global time-averaged heat transfer for various excess gas velocities and pressures.

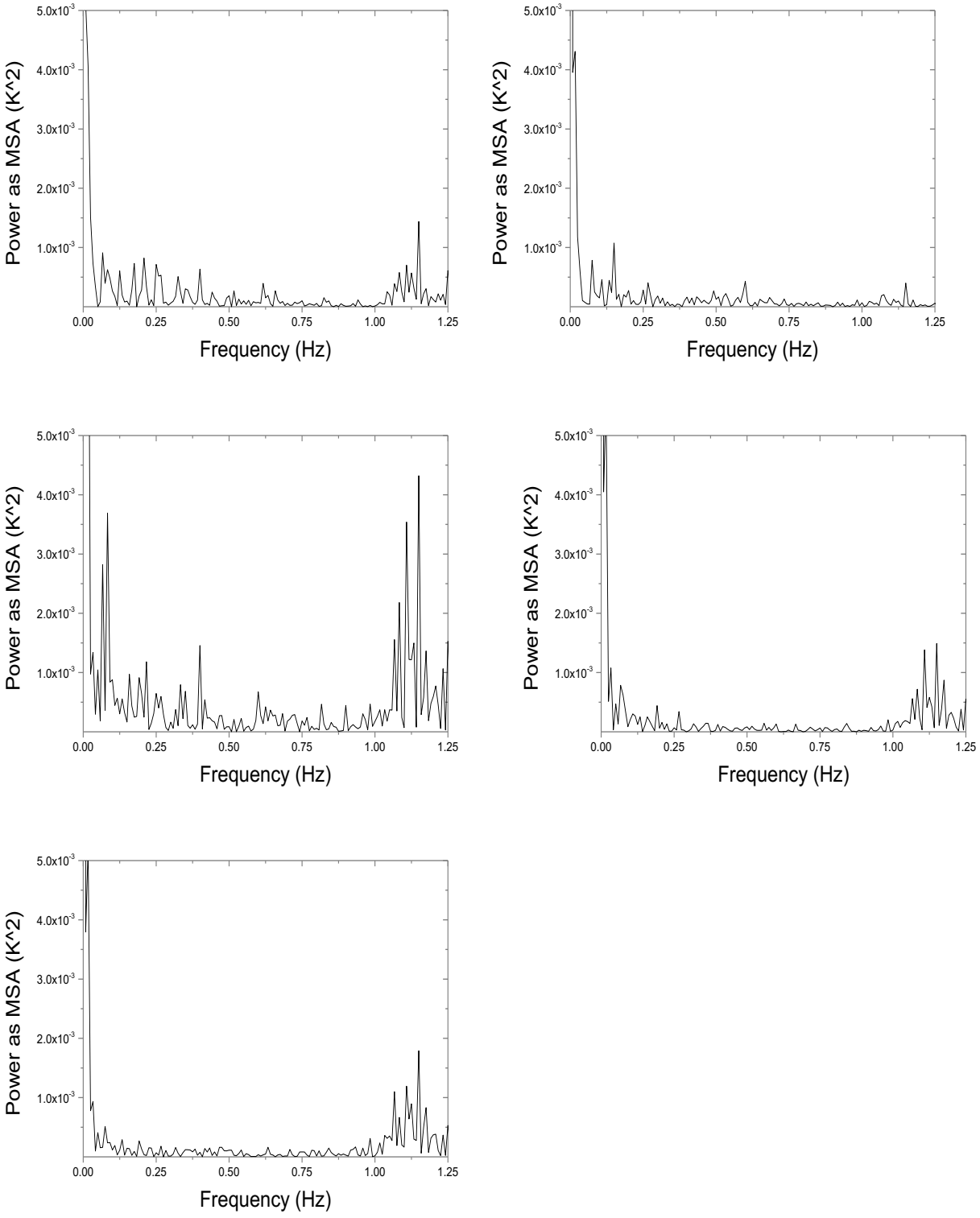

Figure 3-12: Power Spectrum of local temperature signal from 1st thermocouple to 5th thermocouple for U_e of 0.29m/s with 9.5kg/h fine particle feed rate at 101 kPa.

3.5.3 Effect of Heating Rod Location within a Tube Bundle

The surface-to-bed heat transfer coefficient was also determined while the heating rod moved from the bottom-row (2nd row) to the inner-row (4th row) in order to investigate the effect of heating rod position within a tube bundle.

As shown in Figure 3-13, the heat transfer coefficient increased as the heating rod was placed higher within the tube bank for fines free experiments at all pressures tested. However, such effect was undermined as pressure increased when fines were present. The heat transfer coefficient increased by 18%, 9% and 6% at 101, 600 and 1200 kPa, respectively. For fines feeding experiments, the heat transfer coefficient increased 17%, 2% and -2% at 101, 600 and 1200 kPa respectively. Moving the heating tube upwards was found having little effect on local heat transfer coefficients as shown in Figure 3-14.

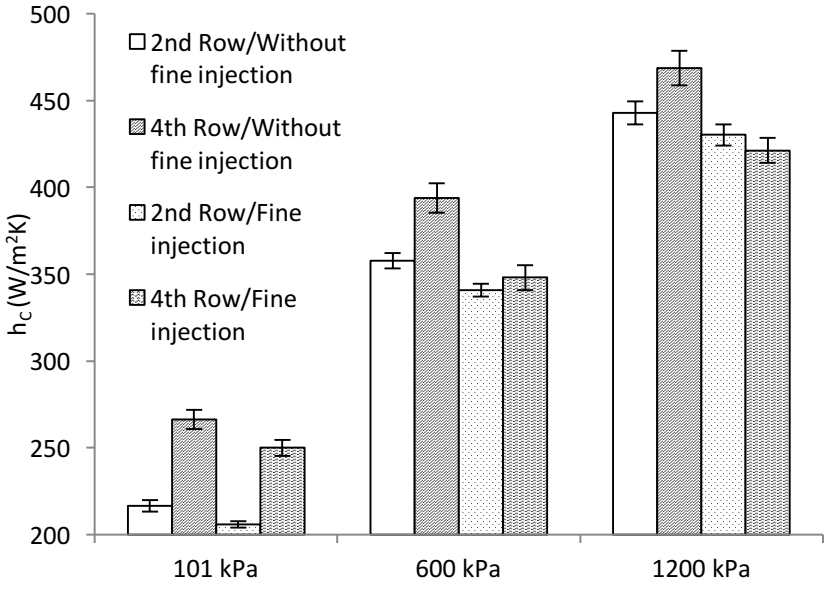

Figure 3-13: Experimental h_C for different heating rod locations (2nd vs 4th row) at U_e = 0.29 m/s and fines feeding rate at 9.5 kg/h.

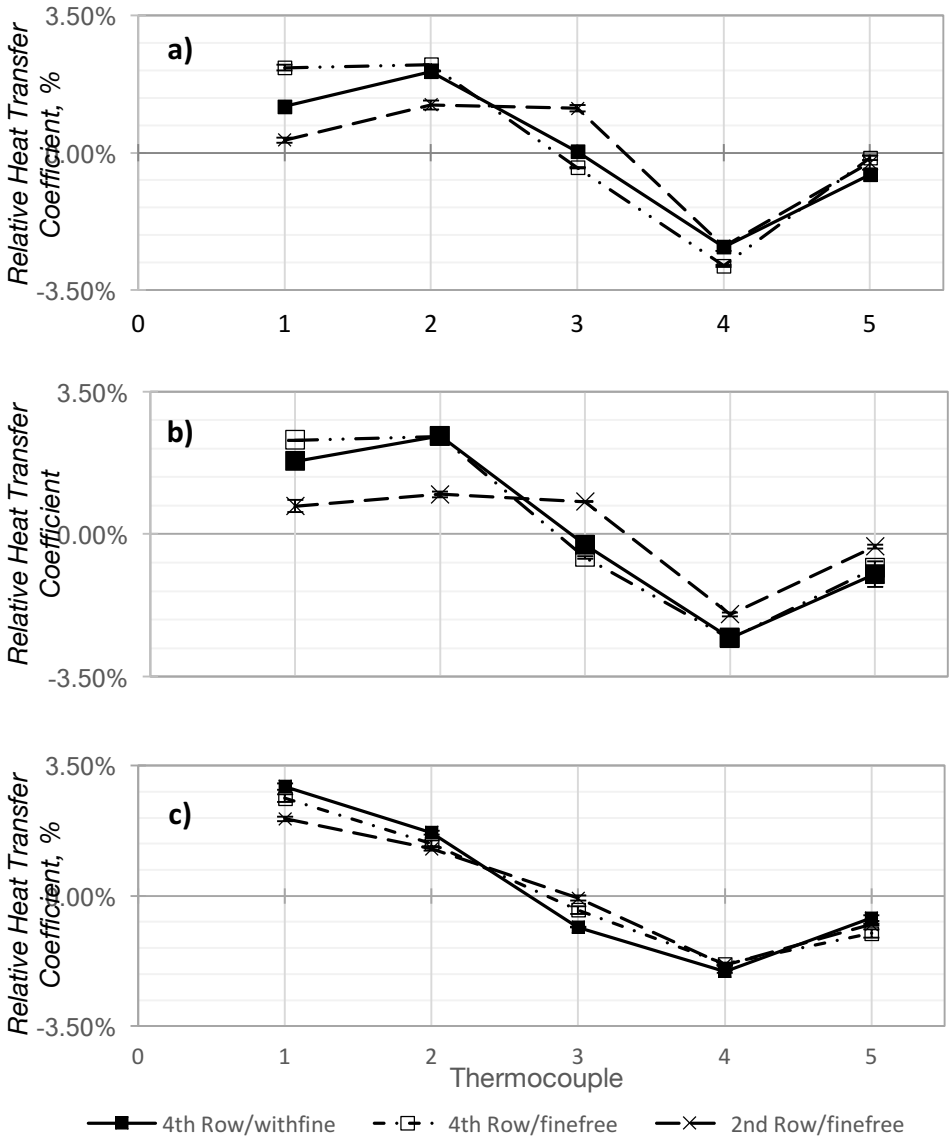

Figure 3-14: Relative heat transfer coefficient across the heating rod surface compared at two locations at a) 1200 kPa, b) 600 kPa and c) 101 kPa at U_e= 0.29 m/s with fine (feed rate at 9.5 kg/h) and without fine injection.

The greater heat transfer coefficient achieved at inner-row tube location could be accounted by the fact that slugs (or large bubbles) were split up by the tubes beneath so that smaller bubbles were contacting with the inner-row tube surface, resulting in a higher particle surface renewal frequency which eventually increased the particle conduction heat transfer. However, this effect would be undermined at elevated pressures since, as discussed in section 3.5.1, bubbles were smaller and

likely passed in-between the tubes instead of hitting them. Moreover, such rise on heat transfer coefficient was also observed at atmospheric condition with presence of fines as heating rod moving upwards. However, no significant increase on heat transfer coefficient was to be found at elevated pressure.

3.6 Conclusions

Oxygen-fired pressurized fluidized bed combustion is considered a promising approach for clean coal combustion. Heat transfer between the bed and a submerged surface is a key design criterion for these intensified operating conditions. As such, cold flow tests were conducted to measure and model the bed-to-surface overall convective heat transfer coefficient at various gas velocities (U_e=0.21, 0.29, 0.51m/s), pressures (101, 600, 1200 kPa), tube positions (2^{nd} and 4^{th} row) as well as with the continuous injection of fine glass particles (D_p = 60 μm) at multiple feed rates (0, 9.5, 14.4 kg/h). The bed material itself were 1 mm glass beads. At the lower heating tube location, both the angular profile around the heating tube and averaged heat transfer coefficients varied as a function of pressure. At atmospheric pressure, the flow was in the slugging regime and the maximum h_C was observed at the bottom of the heating tube, whereas it moved to the side of the tube at high pressure as a bubbling regime occurred. Moreover, the averaged heat transfer coefficient approximately doubled from 101 to 1200 kPa. The average heat transfer coefficients within the fluidized bed matched the comprehensive correlation from Molerus et al. [29] within a 5% difference across all conditions when fines were not present. The addition of fine particles, forming up to 5% of bed mass, decreased the average overall heat transfer coefficient by 10 ~ 20 W/m^2 K and there was no significant effect on the angular profile across the tube surface. The mechanism of such requires further investigation with a reduction in the gas-phase turbulence being a probable cause. Varying the heating tube position from the bottom-row (2^{nd} row) to the

inner-row (4^{th} row) was influential when the gas bubble dynamics were affected the most. The average overall heat transfer coefficient increased by 6 to 18% for fine free experiments, although the extent of the increase was lessened as the pressure increased. In the presence of fines, location of the heating tube was found to be important at atmospheric condition since h_C increased but as the pressure was elevated no significant difference was observed.

3.7 Acknowledgement

Financial support from the Natural Sciences and Engineering Research Council (NSERC) of Canada, and financial assistance and input from NRCan CanmetENERGY-Ottawa and Gas Technology Institute-GTI (USA) are acknowledged with gratitude.

References

[1] S.A.Y. W. Follett, M. A. Fitzsimmons, S. V. Pisupati, C. G. Sonwane, S. Jovanovic, T. W. Manley, D. Hiraoka, Development of a pilot scale coal coal powered oxy-fired pressurized fluidized bed combustor wity CO_2 capture, in: Power-Gen Eur. Conf., 2015.

[2] L. Chen, S.Z. Yong, A.F. Ghoniem, Oxy-fuel combustion of pulverized coal: Characterization, fundamentals, stabilization and CFD modeling, Prog. Energy Combust. Sci. (2012).

[3] J. Hong, G. Chaudhry, J.G. Brisson, R. Field, M. Gazzino, A.F. Ghoniem, Analysis of oxy-fuel combustion power cycle utilizing a pressurized coal combustor, Energy. 34 (2009) 1332–1340.

[4] J. Hong, R. Field, M. Gazzino, A.F. Ghoniem, Operating pressure dependence of the pressurized oxy-fuel combustion power cycle, Energy. 35 (2010) 5391–5399.

[5] P. Basu, Combustion and gasification in fluidized beds, CRC Press (2006).

[6] J.S.M. Botterill, Fluid-bed heat transfer. Gas-fluidized bed behaviour and its influence on bed thermal properties, (1975).

[7] J.R. Grace, Fluidized bed heat transfer, Handb. Multiph. Flow, McGraw-Hill, Hemisphere, Washington, DC. 970 (1982).

[8] J.C. Chen, J.R. Grace, M.R. Golriz, Heat transfer in fluidized beds: Design methods, Powder Technol. (2005).

[9] O. Molerus, K.-E. Wirth, Heat transfer in fluidized beds, Springer Science & Business Media, 11 (2012).

[10] I. Sidorenko, M.J. Rhodes, Pressure Effects on Gas-Solid Fluidized Bed Behavior Pressure Effects on Gas-Solid Fluidized Bed Behavior, 1 (2003).

[11] A.M. Xavier, J.F. Davidson, Heat transfer in fluidized beds, AIChE Symp. Ser. 77 (1985) 368-373.

[12] Q.F. Hou, Z.Y. Zhou, A.B. Yu, Gas-solid flow and heat transfer in fluidized beds with tubes: Effects of material properties and tube array settings, Powder Technol. 296 (2016) 59–71.

[13] S.E. Olsson, J. Wiman, A.E. Almstedt, Hydrodynamics of a pressurized fluidized bed with horizontal tubes: influence of pressure, fluidization velocity and tube-bank geometry, Chem. Eng. Sci. 50 (1995) 581–592.

[14] S.S. Zabrodsky, Y.G. Epanov, D.M. Galershtein, S.C. Saxena, A.K. Kolar, Heat transfer in a large-particle fluidized bed with immersed in-line and staggered bundles of horizontal smooth tubes, Int. J. Heat Mass Transf. 24 (1981) 571–579.

[15] S.W. Kim, J.Y. Ahn, S.D. Kim, D. Hyun Lee, Heat transfer and bubble characteristics in a fluidized bed with immersed horizontal tube bundle, Int. J. Heat Mass Transf. 46 (2003) 399–409.

[16] A.O.O. Denloye, J.S.M. Botterill, Bed to surface heat transfer in a fluidized bed of large particles, Powder Technol. 19 (1978) 197–203.

[17] J.S.M. Botterill, M. Desai, Limiting factors in gas-fluidized bed heat transfer, Powder Technol. 6 (1972) 231–238.

[18] A.I.P. V.A. Borodulya, V.L. Ganzha, Heat transfer between fluidized bed of large particles and horizontal tube bundles at high pressures, Int. J. Heat Mass Transf. 27 (1984) 1219–1225.

[19] R. Chandran, J.C. Chen, F.W. Staub, Local heat transfer coefficients around horizontal tubes in fluidized beds, J. Heat Transfer. 102 (1980) 152–157.

[20] S.C. Saxena, V.L. Ganzha, Heat transfer to immersed surfaces in gas-fluidized beds of large particles and powder characterization, Powder Technol. 39 (1984) 199–208.

[21] S.C. Saxena, N.S. Grewal, J.D. Gabor, S.S. Zabrodsky, D.M. Galershtein, Heat transfer between a gas fluidized bed and immersed tubes, Adv. Heat Transf. 14 (1979) 149–247

[22] L.R. Glicksman, M.R. Hyre, P.A. Farrell, Dynamic similarity in fluidization, Int. J. Multiph. Flow. 20 (1994) 331–386.

[23] W. C. Yang, M. Dekker, Handbook of fluidization and fluid-particle systems, CRC Press (2003).

[24] D.G. Karamanev, Equations for calculation of the terminal velocity and drag coefficient of solid spheres and gas bubbles, Chem. Eng. Commun. 147 (1996) 75–84.

[25] R. Turton, O. Levenspiel, A short note on the drag correlation for spheres, Powder Technol. 47 (1986) 83–86.

[26] M. Liu, Y. Zhang, H. Bi, J.R. Grace, Y. Zhu, Non-intrusive determination of bubble size in a gas-solid fluidized bed: An evaluation, Chem. Eng. Sci. 65 (2010) 3485–3493.

[27] J.S.M. Botterill, M. Desai, Limiting factors in gas-fluidized bed heat transfer, Powder Technol. 6 (1972) 231–238.

[28] W. Prins, Fluidized bed combustion of a single carbon particle, (1987).

[29] O. Molerus, A. Burschka, S. Dietz, Particle migration at solid surfaces and heat transfer in bubbling fluidized beds -- II. Prediction of heat transfer in bubbling fluidized beds, Chem.

Eng. Sci. 50 (1995) 879–885.

[30] V.A. Borodulya, V.L. Ganzha, A.I. Podberezsky, Heat transfer berween fluidized bed of large particles and horizontal tube bundles at high pressures, Int. J. Heat Mass Transf. 27 (1984) 1219–1225.

[31] J.A. Doherty, S.C. Saxena, Heat Transfer from Horizontal Tube Bundle in a Gas-Fluidized Bed, Proc. Eighth Int. Conf. Fluid. Combust., (1985) 1389–1398.

[32] G. Flamant, J.D. Lu, B. Variot, Towards a generalized model for vertical walls to gas—solid fluidized beds heat transfer—II. Radiative transfer and temperature effects, Chem. Eng. Sci. 48 (1993) 2493–2503.

[33] K.J.K. Buettner, C.D. Kern, The determination of infrared emissivities of terrestrial surfaces, J. Geophys. Res. 70 (1965) 1329–1337.

[34] S. Oka, Fluidized bed combustion, CRC Press (2003).

[35] T. Khan Truton, R., The measurement of instantaneous heat transfer coefficients around the circumference of tubes immersed in a high temperature fluidized bed, Int. J. Heat Mass Transf. 35 (1992).

[36] S.E. Olsson, Local instantaneous and time-averaged heat transfer in a pressurized fluidized bed with horizontal tubes: Influence of pressure, fluidization velocity and tube-bank geometry, (1995) 3231–3245.

[37] A.W. Vreman, Turbulence characteristics of particle-laden pipe flow, J. Fluid Mech, (2007) 584

Chapter 4 Conclusions and Recommendations for Future Work

It is evident that clean fossil fuel combustion technologies are necessary as climate change becomes increasingly severe and the total worldwide energy consumption increases significantly. The oxygen-fired pressurized fluidized bed combustion is a promising technology in achieving near-zero GHG emissions before alternative energy sources being able to reliably produce significant amount of energy. A 1 MW_{th} pilot plant Oxy-PFBC has been built and is currently under operation at NRCan CanmetENERGY in Ottawa, Ontario, Canada to evaluate the feasibility of such technology. Supplementary experimental data and information were essential and thus were provided by this work in relation to the bed-to-surface heat transfer at the intensified operating conditions of the Oxy-PFBC pilot plant. Local and global heat transfer coefficients were determined at various pressures and gas velocities, with and without addition of fines, using a specific in-bed tube bundle arrangement. The cold-flow experiments were carried out in a pilot-scale pressurized fluidized bed which enabled continuous addition of fines. This not only, simulated similar conditions to that of the Oxy-PFBC but also provided novel information about systems of binary mixture of small and large particles.

Results revealed that the bed-to-surface heat transfer coefficient nearly doubled from 101 kPa to 1200 kPa at a constant excess gas velocity. This confirms that the real Oxy-PFBC will benefit from high pressure conditions. As pressure was increased, the fluidization flow regime switched from slugging to bubbling, which was confirmed by the time-series analysis of bed pressure drop signals and local relative temperature signals. The highest local heat transfer coefficient occurred at the side of the tube in bubbling regime (elevated pressure conditions) whereas the local peak happened

at the bottom of the tube at slugging regime (atmospheric condition). This finding could be used in erosion analysis for the real process. Increasing gas velocities was found to slightly affect both global and local heat transfer coefficients. Moving the heating surface from bottom-row to inner-row (2^{nd} to 4^{th} row) was found to increase bed-to-surface heat transfer coefficient by 6 to 18% in both atmospheric and elevated pressure conditions while little impact on local angular profile was observed. As gas bubbles are being split up at the bottom-row tube, smaller gas bubbles are contacting the inner-row heating rod which in turn results in a greater particle surface renewal frequency. Thus a greater particle conduction heat transferis achieved.

Addition of fines led to a slight reduction in bed-to-surface heat transfer coefficient. A 0.5 to 5% mass fraction of fine particles present in the bed across all conditions resulted in a decline of averaged overall heat transfer coefficient by10 ~ 20 W/m^2 K. Such small amount of fine particles inside the bed was believed to reduce the gas turbulence and thus reducing the contribution from the gas convection heat transfer. For the operating conditions tested in this work, Molerus et al. [3] model was found to provide a close prediction of the overall convective heat transfer coefficient found experimentally.

Further research on bed-to-surface heat transfer could be conducted in two areas. The bed material could be changed from Geldart Group D to Group B particles. It will be easier to achieve bubbling regime at atmospheric conditions for fluidized beds of Geldart B particles as the difference between minimum bubbling velocity and minimum slugging velocity becomes greater. With a smoother fluidization, a greater bed-to-surface heat transfer coefficient will be achieved. It will also be of interest to investigate the bed-to-surface heat transfer coefficient for a bimodal particle mixture where both heat transfer mechanisms are dominated by particle conduction. Finally, it will be of interest to investigate the effect of tube spacing. It is worth to have a horizontal staggered

tube bundle with an equilateral triangle tube arrangement where the heating rod is surrounded by 6 other tubes with the same distance. The pitch between tubes and the heating rod could be considered as an independent variable. The intensive tube arrangements could cause severe problems in commercial facilities (e.g., creating dead zones resulting in particle accumulation) and thus the effect of tube spacing on heat transfer is of important.

Reference

[1] IEA, CO_2 Emissions from Fuel Combustion 2017, OECD Publishing, (2017).

[2] S.A.Y. W. Follett, M. A. Fitzsimmons, S. V. Pisupati, C. G. Sonwane, S. Jovanovic, T. W. Manley, D. Hiraoka, Development of a pilot scale coal coal powered oxy-fired pressurized fluidized bed combustor wity CO_2 capture, Power-Gen Eur. Conf., (2015).

[3] O. Molerus, A. Burschka, S. Dietz, Particle migration at solid surfaces and heat transfer in bubbling fluidized beds -- II. Prediction of heat transfer in bubbling fluidized beds, Chem. Eng. Sci. 50 (1995) 879–885.

Appendix A: Detailed Picture of High-pressure Fluidization Apparatus

The high-pressure apparatus for bed-to-surface heat transfer experiments is consisting of three major systems, which are gas-solid fluidized bed column, fine particle storing and conveying system and two parallel filters.

Figure A-1. High-pressure fluidization column

Figure A-2. Pressure vessel containing auger feeder

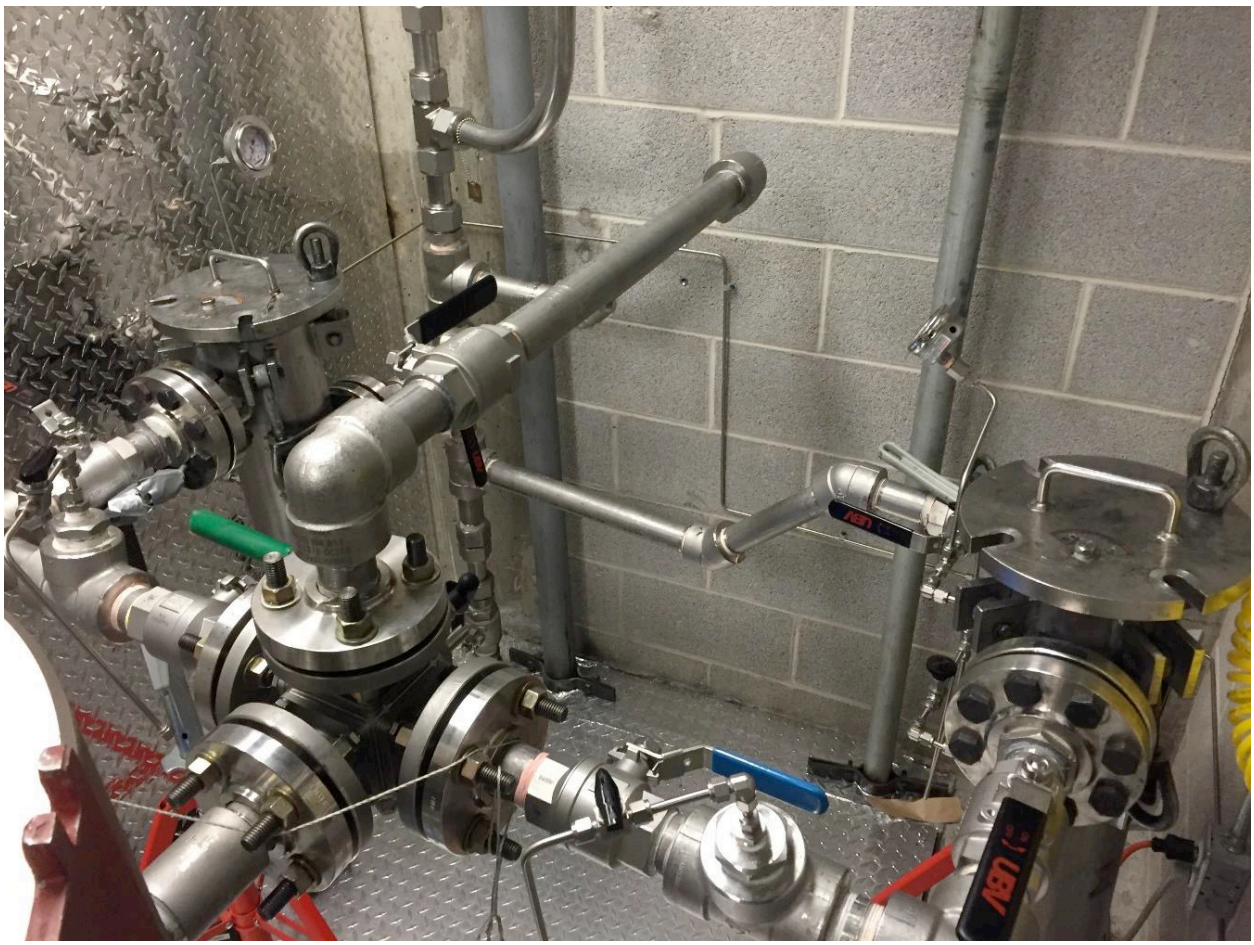

Figure A-3. Two parallel filters

Appendix B: Results for Gas-only Experiments

Gas-only experiments were operated under an equal superficial gas velocity of 1.08 m/s and 0.74 m/s for with bed experiment at pressure of 101 kPa and 1200 kPa respectively.

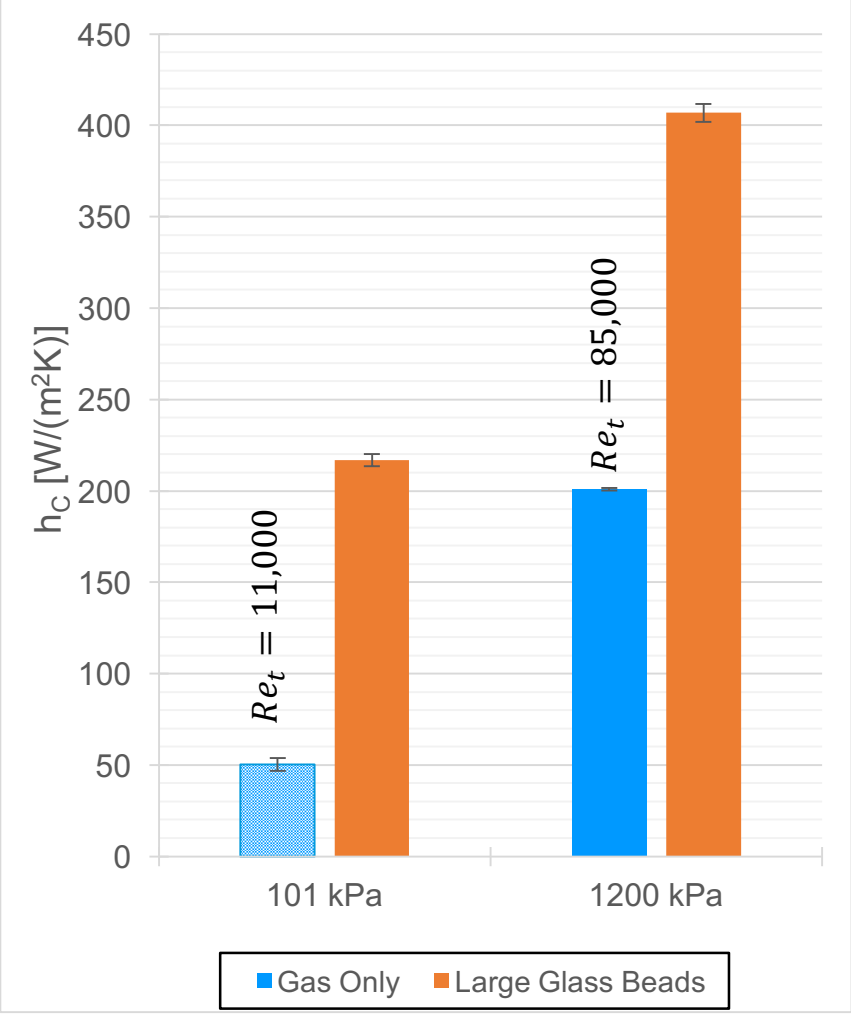

Figure B-1. Overall convective heat transfer coefficient for gas-only and large glass beads only experiments

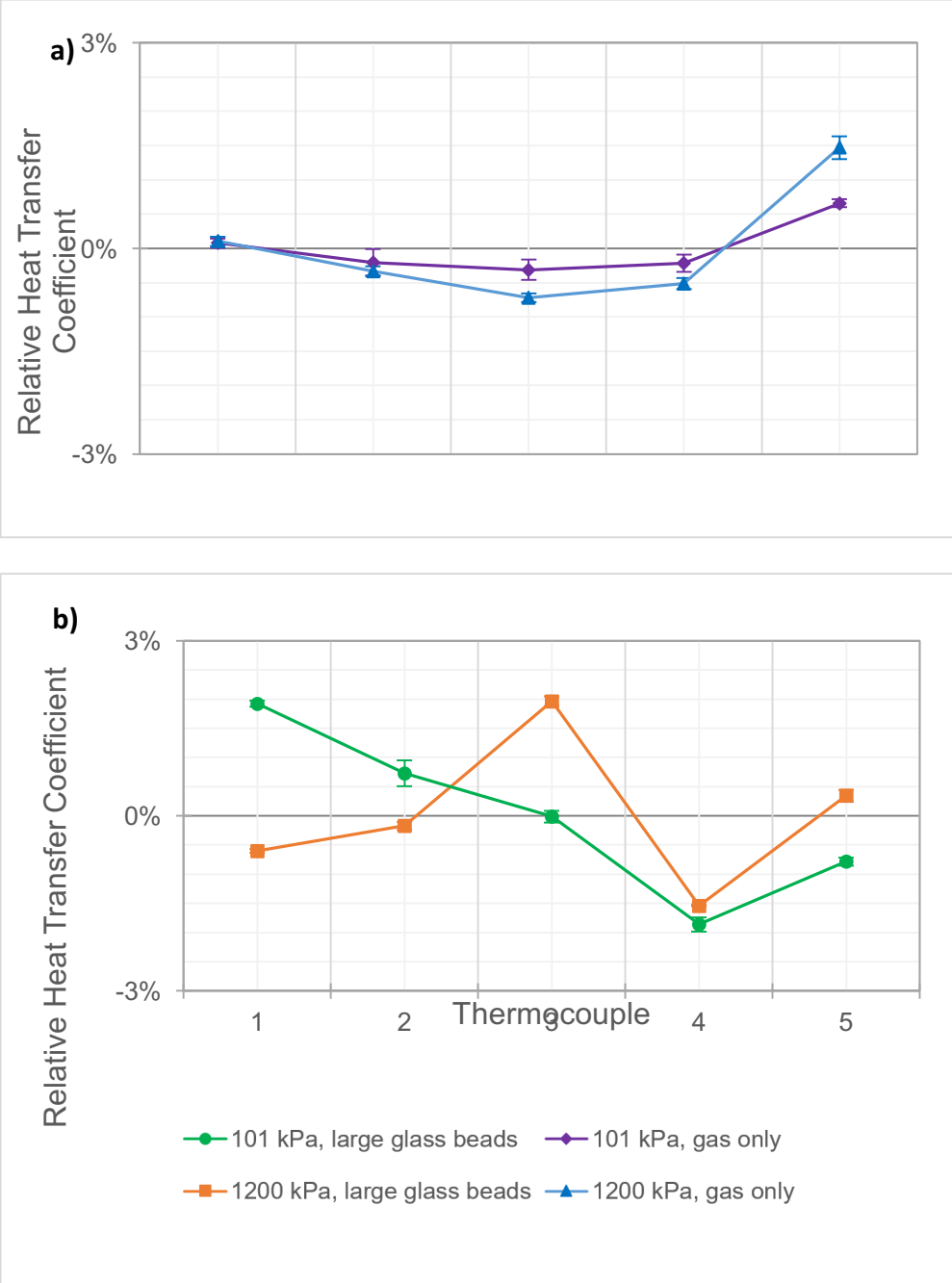

Figure B-2. Local relative heat transfer coefficient for a) gas-only experiments; b) large glass beads only experiments